Cape Peninsula
University of Technology

EXPERIMENTAL AND NUMERICAL INVESTIGATION OF HEAT TREATMENT OF Al-Si-Cu ALLOY

LLEWELLYN HEINRICH CUPIDO

Dissertation submitted in fulfilment of the requirements for the degree
Master of Technology: Mechanical Engineering
in the Faculty of Engineering
at the Cape Peninsula University of Technology

Supervisor: Dr N Mahomed

Co-supervisor: Dr PL Zak

September 2014

DECLARATION

This dissertation is part of a double degree programme between the Faculty of Engineering of Cape Peninsula University of Technology (South Africa) and the Faculty of Foundry Engineering of AGH University of Science and Technology (Poland).

As part of the programme, the student completed the following courses at Cape Peninsula University of Technology:

COURSEWORK: STL500S: Continuum Mechanics and Intro to Finite Element Analysis MTD500S: Metallurgical Thermodynamics
COMPUTER AIDED DESIGN: Introduction to CATIA. One-week training programme at the Product Lifecycle Management Competency Centre, CPUT.
PATTERN MAKING IN FOUNDRY TECHNOLOGY: Principles of additive manufacturing and rapid prototyping. Rapid Pattern-Making of wax models for sand and investment casting. One-week programme conducted at the RPD Laboratory, University of Stellenbosch.
FOUNDRY TECHNOLOGY: SAND CASTING: Principles of Sandcasting. One-week internship programme conducted at Atlantis Foundries.
FOUNDRY TECHNOLOGY: INVESTMENT CASTING: Physical Aspects of Castings (Mould, Production, Materials, Solidification of Metals); Wax room process review (Wax room operations, Materials, Production work); Ceramic Shell room review (Shell room operations, Materials, Production work); Melting and casting review (Ceramic mould preparation, Ferrous and non-ferrous melting, Spectrographic analysis and casting). One-week programme conducted at the CASTCO Foundry.
SIMULATION OF CASTING PROCESSES: Introductory course on the use of MAGMASOFT: Process Modelling; Mesh Generation; Process Simulation.
Eight-week Product Design and Simulation project using CATIA and MAGMASOFT.

As part of the programme, the student completed the following courses at AGH University of Science and Technology:

Coursework:	ECTS
Mathematics for Engineers	3
Thermodynamics of Alloys	3
Theory of Foundry Processes	3
Physical Chemistry of Metallurgical and Foundry Processes	3
High Quality Iron Alloys	2
Nonferrous Alloys for Special Applications	2
Metal Matrix Composites	2
Metal Forming Products	3

Powder Metallurgy Products	2
Designing of CAMD Products	2
Finite Difference Methods	3
Applying CAD Systems for Design Casting Technology	2
Foreign Language (special)	3
Theory of Elasticity and Plasticity	3
Iron Alloy Castings	2
Nonferrous Alloy Castings	2
Numerical Simulation and Experimental Methods for Mechanical Characterisation of Solids	4
Computer Networks and Clusters	2
Applying Computer Methods to Optimise a Cast Strength	2
Object Oriented Programming and Database Programming	2
Design and Application of Advanced Engineering Materials	2
Multi-scale Modelling	2
Precision Casting Technology	2
Computer Aided Tooling Manufacturing for Foundry Engineering	2
Elective Course I: Casting Technology Design	1
Elective Course I: Developing Quality of the Surface Layer of Castings	1
Metrology of Foundry Processes	1
Art Casting Technology	2
Selected Aspects of Corrosion in Cast Materials	2
Designing of Information Systems for Production Management in Foundries	1
Numerical Simulation and FEM	3
Seminar	1
Project	10

I, Llewellyn Heinrich Cupido, declare that the contents of this dissertation represent my own unaided work, and that the dissertation has not previously been submitted for academic examination towards any qualification outside of the double degree programme. Furthermore, it represents my own opinions and not necessarily those of the Cape Peninsula University of Technology.

Signed **Date**

ABSTRACT

Aluminium alloys has seen recent increase usage in the automotive industry. This is due to the global obligation towards carbon emission reduction and fuel efficiency in the transport sector. The good strength-to-weight ratio offered by Al-Si-Cu alloys showed promising results towards the compliance of these environmentally friendly criteria.

The enhanced mechanical properties is obtained when the alloy is subjected to the T6 heat treatment process, which cause microstructural changes due to the evolution of intermetallic phases. The process involves solution heat treatment, for dissolving soluble Cu- and Mg-containing phases, the homogenization of alloying elements, and the spheroidisation of eutectic Silicon. It is followed by quenching, for maximum precipitation hardening particle retention in solution, and a further artificial ageing process with the aim to acquire a uniform distribution of small precipitates, for strength improvement.

The heat treatment schedule applied in this study was conducted as follows: Solution heat treatment at a temperature of 525°C for 6h Quenching in water of temperature 50°C; Artificial ageing for 8h at a temperature of 175°C, and then after left inside furnace to cool down to room temperature. This is higher than the 520°C, but shorter than the 8-12h, observed in literature. Also, quenching is done at a lower temperature rather than 60°C, and artificial ageing at a higher temperature, rather than the 155°C. This was done to be able to draw a comparison between the MAGMASOFT® simulation, which has this non-adjustable schedule, and the experimental results.

The simulated and experimental results were comparable and similar outcomes, but with some discrepancies. Such as the porosity was far more visible and intense in the experimental, than what was predicted by the software. The as-cast and heat treated microstructure revealed the expected evolution of intermetallic particles, such as dissolving of the Al_2Cu and the spheroidisation of the eutectic Si phases. Another phase that was identified was the insoluble AlFeSi and other possible Fe-containing phases, which due to the higher solution heat treatment temperature, showed partial fragmentation and dissolution.

The study provided practical data about the effect of heat treatment on microstructural evolution and how it affects the properties of the Al-Si-Cu alloy. It also brought to the attention and understanding of how critical pouring temperature is, as it affect the initial nucleation, and cooling rate, and therefore the micro and macro properties.

ACKNOWLEDGEMENTS

I would like to express my sincere gratitude to:

- Dr Nawaz Mahomed and the RIFT (Research and Innovation in Foundry Technology) project, for allowing me this study opportunity and financial support, and the subtle words of motivation

- Prof. Krajewski for acceptance to the faculty and provision to the facilities at the university

- Dr Ewa Olejnik (PhD Eng.) for assisting with the XRD examination and data analysis

- Mr Grzegorz Piwowarski (MSc)for helping with preparation of the castings and heat treatment

- Ms Beata Gracz (MSc)for helping during samples preparation, and providing the appropriate literature

- Dr Zbigniew Szklarz (PhD Eng.) for helping with the microstructural analysis.

- Mr Marek Momot (MSc), from KomOdlew, for with assistance with MAGMASOFT® and simulations of my casting

- Dr Paweł Leszek Żak for his supervision and always making time in his hectic schedule, to discuss concerns and ideas. Also, for dealing and handling the “behind the scenes” administrative work, for which I was unaware of

DEDICATION

To my dearest parents, Gerald and Kathleen Cupido

For their enduring support and believe in me, I hope this makes you proud.

Table of Contents

Nomenclature

C_L	Element concentration in liquid (%wt)
C_0	Initial concentration of element (%wt)
D_s	Diffusion coefficient in solid (m^2/s)
f_s, g_α	Volumetric solid fraction
i	Solute element index (copper, silicon)
k	Equilibrium partition coefficient
L	Length scale of microsegregation domain
m	Slope of liquidus line (°C)
t_f	Local solidification time (s)
T_{liq}	Liquidus temperature (°C)
$\dot{T}_{\mathrm{liq}}$	Cooling rate (°C/s)
T_{pure}	Melting temperature of pure aluminium (= 660.3°C)
T_{sol}	Solidus temperature (°C)
α, β	Solid phases
β_i	Back-diffusion parameter
α_i	Fourier number of solute i
α^+	Fourier number accounting for coarsening
α^c	Extra back-diffusion from coarsening $(= 0.1)$
λ_2	Secondary dendrite arm spacing (µm)
ξ	Dimensionless *x*-coordinate
τ	Dimensionless time

Glossary

FDM – Finite Difference Method (Euler method), a numerical technique for solving differential equations

Friedel effect – Small and not too hard precipitates are normally sheared by moving dislocations

GP zones – Guinier-Preston zones fine-scale metallurgical phenomenon, involving early stage precipitation

HPDC – High Pressure Die Casting

MAGMASOFT® – a commercially available software for foundry casting simulations

Orowan mechanism – when the movement of dislocation bypasses the precipitates by bowing, due to the precipitates being harder and bigger

Ostwald ripening – an occurrence in solid solutions or liquid sols (colloidal suspension of very small solid particles) that describes the change of an inhomogeneous structure over time, i.e., small crystals or sol particles dissolve, and redeposit onto larger crystals or sol particles.

SDAS – Secondary Dendrite Arm Spacing

SEM – Scanning Electron Microscopy

SOLIDWORKS – 3D Computer Aided Draughting software by Dassault Systèmes S.A.

STL – a stereolithography file format created by a CAD software that is supported by many other software packages

TEM – Transmission Electron Microscopy

UTS – Ultimate Tensile Strength

wt% – mass fraction as a percentage or weight percentage, which is the compositional ratio of a substance within a total mixture

YS – Yield Strength

XRD – X-ray Diffraction

Chapter 1. Introduction

1.1. Overview

The use of aluminium alloys has seen an upward trend in recent times especially in the automotive industry. This is due to the need to use parts that are lightweight offering the advantages of reduction in fuel consumption, performance improvements while maintaining high safety requirements, and the need to adhere to governmental environment regulations [1, 2, 3].

Despite the application of aluminium alloys in other parts of the vehicle, such as extrude sheet metal for the body, engine blocks and cylinder heads, the heaviest components of the automobile make use of aluminium cast alloys to meet the economic and ecological demands [4, 5, 6]. This is because weight reduction can lead to smaller engines with the same performance output, which enables the usage of reduced transmissions and smaller fuel tanks. It is estimated that 10% of vehicle mass decrease results in 8–10% of fuel consumption improvement, which in turn means less emissions [1, 2].

Heat treatment is important for the improvement of the material properties of Al-Si-Cu alloys. Many earlier studies into the thermal processing has been conducted, but emphasis only on a particular feature of the whole procedure. A complete investigational study taking into account all the stages of the thermal treatment is still required [7]. In the review of Sjölander and Seifeddine [8], they conclude the importance of considering the entire treatment process to ensure the optimum material properties.

Furthermore, according to Mohamed and Samuel [7], model development for microstructure prediction and changes in material property in aluminium alloys has been mostly concentrated on wrought alloys. Integrated models for microstructural evolution during solution thermal treatment and its effect on the ageing process have been disregarded.

1.2. Problem statement

Al-Si-Cu alloys presents opportunities for weight reduction in automotive applications, besides other high-technology applications. This is partly due to enhanced mechanical properties induced by Silicon and Copper.

For such components produced by sandcasting (or HPDC), there is a need to improve the microstructure through heat treatment. This is to reduce the chemical inhomogeneity due to

microsegregation, which generally leads to a reduction in mechanical properties of the material.

1.3. Research Objective

This study involves the investigation of the improvement in microstructure of Al-Si-Cu alloys under varied heat treatment regimes. The analysis will be further corroborated through numerical simulations using casting simulation software (MAGMASOFT®), with the aim of developing thermo-mechanical-metallurgical properties for use in the simulation process.

This study will lead to a general know-how of heat treatment of non-ferrous alloys and their associated microstructural evolution, as well as the numerical modeling of microsegregation in Al-Si-Cu alloys.

1.4. Facilities

The Foundry Technology Research Group in the Faculty of Engineering at CPUT is a relatively new development. Together with the Product Lifecycle Management Competency Centre (PLMCC), it provides a full design through simulation capability using design tools such as CATIA and MAGMASOFT for simulation of casting processes.

The Faculty of Foundry Engineering, at the AGH University of Science and Technology, in Krakow, Poland, has facilities for sand casting, and a heat treatment furnace that is able to dissolve and homogenize aluminium alloys. The Faculty has a laboratory for metrology and microstructural analysis (optical and scanning electron microscopy), and the capability to conduct Differential Scanning Calorimetry. They also have several software packages, with full licenses, to determine metallurgical properties such as Thermo-Calc for the development of phase diagrams.

Chapter 2. Literature Review

2.1. Application of Al-Si-Cu alloys

The aluminium-silicon (Al-Si) alloys, which also contains copper (and/or magnesium), are commercially known as A319.0 (ISO: AlSi6Cu4). It is a popular alloy for various applications such as automotive cylinder heads, internal combustion engine crankcases, and applications where good casting characteristics, pressure tightness and moderate strength are required. This is due to the combination of exceptional properties such as low coefficient of thermal expansion, fluidity, high wear resistance, good corrosion resistance, high strength to weight ratio and good machinability in foundry products [3, 4].

Table 2.1: Thermal Properties of Alloy 319.0 *[4]*

Property	**Temperature (°C)**
Liquidus	605
Solidus	515
Melting	675 to 815
Casting (Sand)	675 to 790

2.2. Composition, microstructure and effects of alloying element

The element composition, with percentage ranges and limits, of a 319.0 type alloy comprises silicon (5.5-6.5%), copper (3.0-4.0%), magnesium (0.1% maximum), iron (1.0% maximum), manganese (0.5% maximum), zinc (1.0% maximum), titanium (0.25% maximum), nickel (0.35% maximum), other (0.5% maximum), and the balance being aluminium [4, 9].

The coarseness of the microstructure is a function of the solidification rate, which also affects the fraction, size and distribution of intermetallic phases, as well as the segregation profiles of solute in the α-Al phase. This minimizes and allows for even distribution of the dendritic arm spacing. Thus, permitting the best properties for an alloy to be obtained. [7]

Silicon affects the alloy by improving the casting characteristics, such as improved fluidity, resistance to hot tear, and feeding characteristics. As an example, increasing the Si content improves fluidity for filling thin walls and intricate designs and shapes [4, 10, 11].

According to Mohamed and Samuel [7], the main phases that originate in the as-cast microstructure of Al-Si alloys are primary α-Al, coarse primary Si, needle like eutectic Si, and other undesirable intermetallic phases.

The second most abundant alloy element, copper (Cu), improves strength and machinability, promotes age hardening and increases interdendritic shrinkage potential. However, it negatively affects the alloys castability, ductility, thermal conductivity, hot tear and corrosion resistance [4, 10, 11, 12]. When combined with nickel, it enhances strength and hardness at elevated temperature [11].

The Al_2Cu phase can exist as dense blocky particles, lamellae eutectic (Al–Al_2Cu) phase, or as a mixture of both, in the as-cast microstructure [13, 14]. This is due to the intermetallic phase that copper forms with Al which precipitates during solidification, and which can be located within the interdendritic regions [13, 14, 15]. During the last stage of solidification, Al_2Cu phases nucleate on coarse eutectic Si particles or on β-Al_5FeSi plates [13, 16, 17]. According to Samuel et al [13], individual fine Al_2Cu particles can also precipitate on top of eutectic Si particles, and presence of nucleation sites, such as Al_5FeSi platelets [7]. It is also stated in [13, 17] that eutectic (Al–Al_2Cu) phases are promoted by high solidification rates [7], while the blocky Al_2Cu phase fraction is increased by Strontium modification [13, 14, 16, 17].

Li et al [16] indicates that if iron is present during solidification, other Cu-containing intermetallics develop, such as Al_7Cu_2Fe or Quaternary-$Al_5Cu_2Mg_8Si_6$.

Magnesium (Mg) can improve the strength and hardness, by allowing hardened through heat treatment. The Mg_2Si phase has a solubility limit of about 0.70% Mg, which beyond no additional strengthening takes place or softening of the matrix occur [4, 10]. The formation of quaternary compound such as $Cu_2Mg_8Si_6Al_5$ is also possible with other elements in the alloy [7].

Iron (Fe) is fundamentally an impurity, and an increase in its content is accompanied by a decrease in ductility. It forms numerous insoluble intermetallic phases, of which $FeAl_3$, $FeMnAl_6$, and AlFeSi, are the most common. Responsible for strength improvement, at elevated temperature, but also causes microstructural embrittlement. Feeding characteristics

are affected negatively with the increase of insoluble phases with respect to iron increase [4, 8, 9].

Cáceres et al. [18] conducted a comparative study to examine the effects of Si, Cu, Mg, Fe, and Mn (manganese), and solidification rate on the material properties of Al-Si-Cu-Mg alloys. They witnessed that the strength is proportional to the content increase of Cu and Mg and reduction in ductility. The increase of Fe also decreased the strength and ductility of low-Si dramatically.

Titanium (Ti) is widely used for grain refinement of aluminium casting alloys, often in combination with smaller amounts of boron [9]. Good grain refiners, such as $TiAl_3$ and TiB_2 [7], are necessary for effective grain refinement, but also concentrations greater than those required for the grain refinement is added to reduce hot cracking tendencies [4, 8]. Also, a new family of grain-refiners, based on the Zn-Ti (zinc-titanium) system, showed hopeful alternatives to the conventional $AlTi_5B$ and $AlTi_3C_{0.15}$ refiners [19, 20].

2.3. Microsegregation

Segregation is defined as the non-uniform distribution of the chemical composition that arise during the solidification process [21, 22, 23]. When it occurs at the cell and dendritic level, it is referred to as microsegregation, which results from accumulation of rejected solute between the growing crystals and its failure, due to either inadequate time or to a physical barrier of solid, to diffuse or mix into the main body of residual liquid [23, 24].

Ghosh [22] states that during solidification, three regions exist, namely solid, liquid and solid–liquid mixture. The solid-liquid region comprises of dendrites and interdendritic liquid, called the mushy zone. Campbell [21] explains that microsegregation occurs when solute is rejected from the solidified dendrites into the liquid interdendritic space, and concentrates in the small regions. This happens due to the dendrite growing into the melt, and as the secondary arms branch from the primary dendrite, the solute is effectively being pushed aside to concentrate in the tiny regions surrounded by the secondary dendrite arms. Elements with the higher melting points are concentrated in the dendrites, and the interdendritic regions have high concentrations of the lower melting point element [25].

Won and Thomas [26] states that the microsegregation stems from the thermodynamic equilibrium solubility differences between the alloying elements that exist in the mushy zone in different phases during solidification.

Microsegregation affects and has implications on the properties of the final casting, and is therefore of technical importance. The formation of brittle non-equilibrium phases can be deleterious to the mechanical properties, poor fatigue behaviour can occur due to concentration variations from an inhomogeneous precipitation distribution after a heat treatment, and corrosion resistance can be affected. Therefore, predictions of microsegregation and microstructure in metallic alloys are very important [26, 27].

2.3.1. Microsegregation models

Stefanescu [28] defines a microsegregation model as a comprehensive theoretical treatment of interface morphology that requires accurate tracking of the solute field during solidification.

Won and Thomas [26] states that most simple microsegregation models assume a relationship between alloy concentration and solid fraction, and a one-dimensional composition profile can be evaluated from this relationship between adjacent dendrite arms (Figure 2.1a). This is due to the complicated dendrite geometry [28].

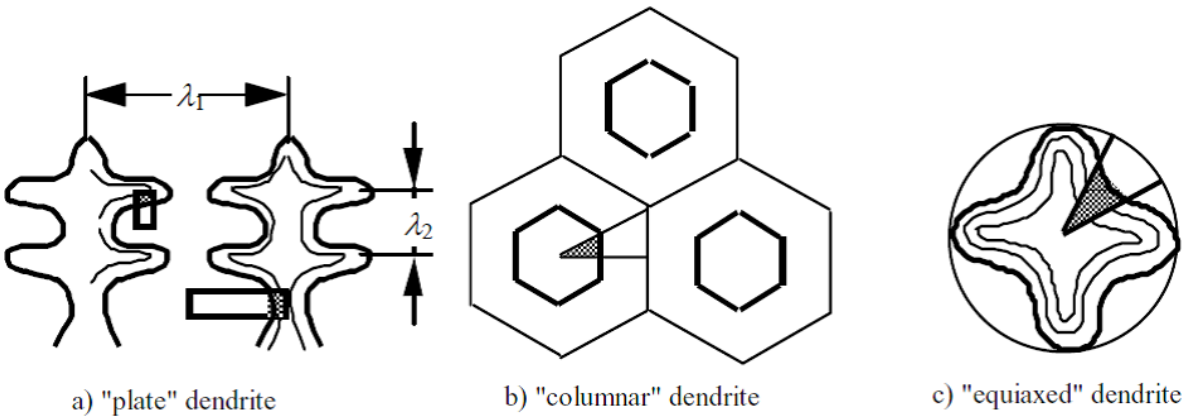

Figure 2.1: Detailed illustration of microsegregation models. (a) One dimensional “Plate” dendrite, (b) 2D columnar dendrite, (c) 3D equiaxed dendrite *[28]*.

The solidification model, called the equilibrium Lever-rule, assumes complete solid-liquid diffusion of all alloying elements:

$$C_{L,i} = \frac{C_{0,i}}{1-(1-k_i)f_s} \tag{1}$$

where $C_{L,i}$ is the liquid concentration of the dissolved element at the solid-liquid interface, $C_{0,i}$ is the original *i*th solute element concentration in the liquid at the interface, k_i is the partition coefficient of the dissolved element, and the volumetric solid fraction is denoted as f_s.

Inaccuracy in the model becomes evident, later during solidification, due to very slow solid phases diffusion, particularly for larger atoms of the solute [26].

Another model, which was first proposed by Gulliver [29], and then later by Scheil [30], known as the Gulliver-Scheil Model, assumes complete liquid diffusion, no solid diffusion, and equilibrium at the solid-liquid boundary (x^*) as the interface progress along the secondary dendritic arm spacing (λ_2), as illustrated in figure 2.2, and mathematically described as [26, 28, 31]:

$$C_{L,i} = \frac{C_{0,i}}{(1 - f_s)^{1-k_i}} \tag{2}$$

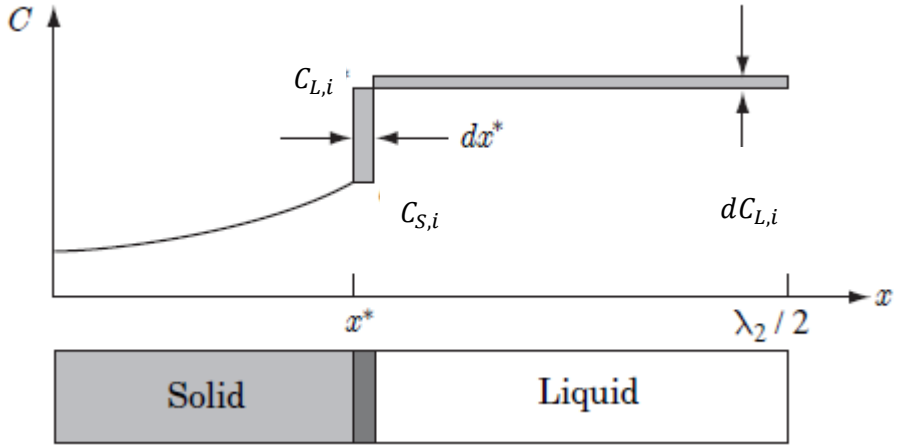

Figure 2.2: A construct demonstrating the partitioning of liquid from the interface *[31]*.

The equation does not adequately estimate the final solute concentration, because at $f_s = 1$, $C_{L,i} = \infty$ [26, 31]. When diffusivity in the solid phase is small, it can be used to calculate microsegregation; however, as stated by Stefanescu [28], that towards the completion of solidification, diffusion of the dissolved matter into the solid phase can influence the microsegregation.

The Brody-Flemings Model [32], which assumes complete diffusion and incomplete back-diffusion in liquid and solid phase, respectively, has the following general form:

This introduces a back-diffusion parameter β_i, which researchers [32, 33, 34] have measured

$$C_{L,i} = C_{0,i}(1 + f_s(\beta_i k_i - 1))^{(1-k_i)/(\beta_i k_i - 1)} \tag{3}$$

in different ways, but the original Brody–Flemings model for a plate dendrite [32],

$$\beta_i = 2\,\alpha_i \quad , \tag{4}$$

where α_i is the Fourier number for the dissolved element i (note that Dantzig and Rappaz [31] uses the symbol Fo to depict the Fourier number, not to it confuse with that of α-phase):

$$\alpha_i = \frac{D_{s,i}\, t_f}{L^2} \tag{5}$$

where $D_{s,i}$ is the diffusion coefficient of the dissolved element i in the solid, the local solidification time, t_f, and L represents the domain length of microsegregation, which is equal to half the SADS (λ_2), see Figure 2.3 [26, 28, 31]:

$$L = \frac{\lambda_2}{2} \quad . \tag{6}$$

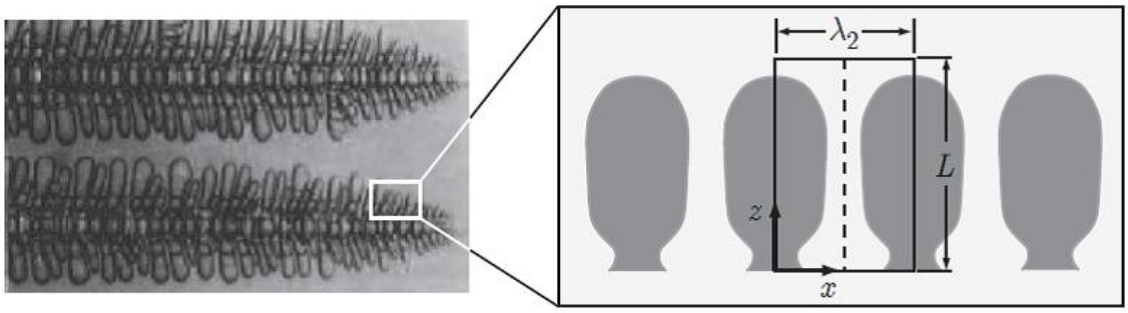

Figure 2.3: (Left) a micrograph of a directionally solidified succinonitrile-acetone alloy. (Right) An idealized segment, displaying a periodic arrangement of secondary dendrite arms. *[31]*

Assuming the known t_f history, Equations (3) through (6) are solved to predict $C_{L,i}$ and related microstructure parameters. When $D_{s,i}$ approaches zero ($\beta_i = 0$) in Equation (3), the Brody–Flemings model reduce to the Gulliver-Scheil equation, and simplifies to the Lever rule when infinitely fast diffusion into the solid phase occurs ($\beta_i = 1$); but when α_i is large and β_i exceeds 1, it becomes not physically reasonable, because there is no conservation of mass [26, 31].

Clyne and Kurz [33] proposed an alteration to ensure the Brody–Flemings model ($0 < \beta_i < 1$) maintain mass conservation, by substituting Equation (4) as follows:

$$\beta_i = 2\alpha_i\left(1 - e^{-\frac{1}{\alpha_i}}\right) - e^{-\frac{1}{2\alpha_i}} \tag{7}$$

Voller and Beckermann [24] added an additional value to the Fourier number. This was to account for the coarsening effect, and was applied as:

$$\alpha_i^+ = \alpha_i + \alpha^C \quad . \tag{8}$$

With this addition, extra back-diffusion could be accounted for, due the actual dendrite arm spacing being smaller before coarsening [26]. It was also shown by Voller and Beckermann [24] that by adopting a constant value of $\alpha^C = 1$, the model is able to forecast the coarsening, for a range of cooling conditions.

Won and Thomas [26] and Stefanescu [28] discuss other models, which can be used for columnar and equiaxed dendrites (Figure 6.1 b and c), and indicate that these models have been implemented into the commercial packages Thermo-Calc [35], IDS [36], and MAGMA [37]. Unfortunately, these models are very computationally intensive. There are also equations such as those proposed by Wołczyński [38] that is a modification of the analogous equation of the Brody-Flemings theory.

Won and Thomas also presents a simple microsegregation model in [16] that resolves Equations (3), (5), and (6) centred on assessing the Clyne–Kurz Model for each dissolved component, as proposed by Ohnaka [34]. This model can be adjusted to change from one dimensional to two dimensional dendrites and, to allow for coarsening as proposed by Voller and Beckermann [24], can be termed as:

$$\beta_i = 2\alpha_i^+ \left(1 - e^{-\frac{1}{\alpha_i^+}}\right) - e^{-\frac{1}{2\alpha_i^+}} \tag{9}$$

where $\alpha_i^+ = 2(\alpha_i + \alpha^C)$ and $\alpha^C = 0.1$.

They [26] also assume for their simple semi-empirical analytical model;

- complete liquid phase diffusion,
- local equilibrium at the solid-liquid interface,
- a constant equilibrium partition coefficient, throughout solidification,
- negligible nucleation undercooling effects, and negligible fluid-flow effects

2.3.2. Secondary Dendrite Arm Spacing (SDAS), Diffusion coefficient, Equilibrium partition coefficient, Local solidification time

Dantzig and Rappaz [31] states that over a range of solidification time, $0.1\,\mathrm{s} < t_f < 10^7\mathrm{s}$, a fairly accurate estimation for λ_2 for Aluminium alloys can be given by: $\lambda_2 \approx$

$\left(10^{-5}\mathrm{m\ s^{-1/3}}\right) t_f^{1/3}$, where the local solidification time (t_f) is obtained, for the assumed constant cooling ($\dot{\mathrm{T}}_{\mathrm{liq}}$) [26]:

$$t_f = \frac{T_{\mathrm{liq}} - T_{\mathrm{sol}}}{\dot{\mathrm{T}}_{\mathrm{liq}}} \tag{9}$$

and the liquidus temperature (T_{liq}), in relation to the composition is given by:

$$T_{\mathrm{liq}} = T_{\mathrm{pure}} - \sum_i m_i \cdot C_{0,i} \tag{10}$$

where T_{pure} ,pure aluminium melting temperature (933 *K*) and m_i is the liquidus line gradient of the individual dissolved components in the Al-phase diagram, shown in Table 2.2 [39].

Rontó and Roósz [40] indicated that copper composition variations, for the Al-Cu-Si alloys, have greater influence on the λ_2 only when the silicon composition is beyond 0.5%. They proposed an equation with greater accuracy to calculate λ_2, that incorporates the collective influence of the local solidification time, t_f cooling rate at liquidus temperature, $\dot{\mathrm{T}}_{\mathrm{liq}}$ copper composition, C_{Cu} and silicon composition C_{Si}:

$$\lambda_2 = 34.9 \cdot {C_{Cu}}^{-0.333} \cdot {C_{Si}}^{-0.145} \cdot {t_f}^{0.208} \tag{11}$$

$$\lambda_2 = 77.09 \cdot {C_{Cu}}^{-1.989} \cdot {C_{Si}}^{-0.078} \cdot {\dot{\mathrm{T}}_{\mathrm{liq}}}^{-0.252} \tag{12}$$

Table 2.2: Physical properties of alloys relevant to solidification [39]

Solutes	**Liquid diffusion coefficient D_L,(m²/s)**	**Solid diffusion coefficient D_S,(m²/s)**	**Partition coefficient k**	**Liquidus slope $-m_L$,(*K*)**
Copper (Cu)	4.9×10^{-9}	1.95×10^{-12}	0.14	260
Silicon (Si)	4×10^{-9}	5×10^{-12}	0.13	600

2.4. Heat Treatment

According to Sjölander and Seifeddine [41], alloy composition and casting process parameters have a major influence on the mechanical properties of cast Al–Si–Cu–Mg alloys, and that through thermal treatment, further enhancement of these properties can occur. They also state that the thermal treatment cycles (temperatures and duration) is dependent on the foundry method, the alloy content and the desired material properties.

The standard heat treatment for Al-Si-Cu alloys, also known as a T6 heat treatment process, is a three-step process. For sand casting the process, as describe by Brooks [42] in the ASM handbook, starts with solution heat treatment at about 505°C (±6°C) for a 12h duration, followed by water quenching at about 65-100 °C. Finally, an aging treatment at a temperature of 155°C for about 2-5h. The tensile yield strength and hardness of a 319.0 alloy is increased from 125MPa to 165MPa and 70HB to 80HB, respectively. All other mechanical properties improves except the elongation, which remains constant, an indication of the ductility of the alloy [4, 43].

Mohamed and Samuel [7] indicates that the improvement of mechanical properties after heat treatment is mainly due to the development of non-equilibrium precipitates within primary dendrites during aging and the Si particles appearances that change from the solution treatment. They also state that Al-Si-Cu alloys have a slow and low age-hardening response as determined by the fraction size, dispersion and consistency of precipitates formed.

2.4.1. Solution heat treatment

In Sjölander and Seifeddine [41, 42] on the study of heat treatment optimisation [8], they stated that solution heat treatment is done at temperatures near to the eutectic temperature, with the aim to dissolve the Cu and Mg containing phases, promote homogeneity in the matrix by the added elements, and spheroidisation of the Si particles.

The rate of the abovementioned processes is proportional to the increase of solution treatment temperature, according to Sjölander and Seifeddine, in their heat treatment review [41]. They also explained that this affects the strength that can be acquired after ageing, due to the increase of solubility of solute into the matrix, because of the higher temperature. They further stated that the maximum solution treatment temperature is dependent on the concentrations of Cu and Mg in the alloy, due to the limitation by incipient melting of phases formed in the interdendritic regions, which is rich in the dissolved elements due to segregation. This causes mechanical properties to reduce due to the resulting distortion caused by the

localised melting. According to Samuel [44], during incipient melting, Cu-containing phases begin to melt at 519°C in an A319 alloy with low-Mg, while for 0.5 wt.% Mg, melting starts at 505°C , due to the presence of Q-$Al_5Mg_8Si_6Cu_2$ phase. The ideal temperatures, before melting occurs, is dependent on the casting solidification rate, which affects the volume fraction, size, morphology and type of Cu-containing phases, and the heating rate to the solution treatment temperature, which affects the time available for dissolution of Cu-containing phases during heating [41].

Han et al [45] states that blocky Al_2Cu phase is difficult to dissolve during solution heat treatment than the eutectic (Al–Al_2Cu) phase, and that fine Al_2Cu phase particles can dissolve within 2h of solid solution heat treatment [7]. Eutectic (Al–Al_2Cu) phase dissolves due to the Al_2Cu particles disintegrating into smaller fragments that can spheroidise, whereby the Cu atoms can dissolve by radial diffusion into the surrounding matrix [16, 45]. Chaudhury and Apelian [46] indicated that the reason for the difficulty in the dissolution of the block-like Al_2Cu phase is because of the lower interfacial area with the matrix and particles elongated uniform profile, and that, according to Han et al [45], takes longer due to it not disintegrating, but dissolving through spheroidisation and diffusion.

According to Moustafa et al. [47], phases like the π-$Al_8Mg_3FeSi_6$ and Q-$Al_5Cu_2Mg_8Si_6$ particles do not dissolve. Crowell and Shivkumar [48] states that Fe-containing phases are difficult to dissolve, like the α-$Al_{15}(Fe,Mn)_3Si_2$ script phase. Although, phases like the β-Al_5FeSi platelets do undergo fragmentation and slow dissolution, but only when subjected to higher temperatures and longer time periods.

In the review of Sjölander and Seifeddine [41], homogenous solid solutions are formed when atoms disconnect from coarser intermetallic phases, and diffuses through the matrix to reduce the concentration gradient. The review also indicates that the time required for homogenisation is dependent on the diffusion rate and the diffusing distance, measured by the secondary dendrite arm spacing (SDAS) [41].

When the solution treatment is too short, not all alloying elements will dissolved, and when it is too long, unnecessary energy usage occurs, as well as remaining Cu-containing particles being affected negatively on the fracture elongation, and Si particles that coarsen, as describe in [8]. This study also indicates that an effective solution heat treatment is determined by the degree of Si spheroidisation, volume fraction, distribution, morphology and composition of phases in the as-cast microstructure, with respect to the solution heat treatment temperature and time selected.

The above study [8] concluded that the coarseness of the microstructure, is a major factor that determines the duration required for solution treatment. The coarser the microstructure the longer the treatment period.

According to Samuel et al. [44] for a 319.2 alloy with SDAS of 22μm, 8h at 515°C or 24h at 505°C was required to dissolve two thirds of the Al_2Cu phase. Dons [49] reported that during solution heat treatment, the β-Fe phase changes into Al_7FeCu_2 phase when a high Cu concentration is present, indicating a loss in Cu in the solid solution to the Al_7FeCu_2 phase.

From the study by Samuel [44], no strength increase was observed by Mg additions to an Al–Si–Cu alloy for solution heat treatment temperature at 480°C, but a 50°C increased reported proportional strength improvement. A two stage solution treatment was investigated by Sokolowski et al. [50], which followed an initial stage at 495°C for 8h, to allow dissolving of the Cu-containing particles, and then proceeded at 520°C for 2h, to allow the alloying elements to homogenise. Increases in strength and ductility were experienced.

According to [41], in an unmodified alloy, Si exists as big brittle fragments, which are responsible for crack formation and have a detrimental effect on alloy ductility, hence the need to spheroidise the eutectic silicon particles. Spheroidisation can occur through long exposure at high temperature, or by additions of Strontium (Sr) to the melt, or both. Eutectic Si particles first fragment, followed by transforming into spheroid and then coarsen, during solution treatment. With additions of Sr, the eutectic Si transform to fibrous, which can be fragment with ease and spheroidise during solution treatment, thus reducing the process time. Required spheroidisation time is dependent on the temperature of solution treatment and the as-cast eutectic Si particles' morphology and size. Crowell and Shivkumar [48] suggested an 8-16h period at 495°C for a 319.1 alloy with Sr additions.

2.4.2. Quenching

The purpose of quenching is to form a low temperature supersaturated solid solution by holding onto the maximum precipitation strengthening elements, while suppressing precipitation; and to retaining an atomic lattice structure with high vacancies [51, 52].

The quench rate is very important for Al-Si alloys, due to the quick formation of precipitates. This is because of the higher supersaturation level and diffusion rate. Between 450°C and 200°C, is the critical temperature range for an effective quench rate [41]. Supersaturation is too low at higher temperatures, and a too low diffusion rate occurs at lower temperatures for critical precipitation [7]. Sjölander and Seifeddine [41] and others [52, 53, 54] observed that a

limiting quench rate of 4°C/s was satisfactory. Exceeding this produce a marginally increase in the yield strength.

According to Mohamed and Samuel [7], an ideal quenching rate is essential to maintain maximum vacancy concentration and reduce part distortion after quenching. Faster rates retain higher vacancy concentration, allowing higher element mobility in the primary Al phase during ageing, but causes higher residual stresses and distortion. A slow rate produces less residual stresses and distortion; however, this causes precipitation that have detrimental effects such as localised over-ageing, grain boundary reduction, higher corrosion tendencies and a reduced response to ageing treatment [55, 56].

Emadi et al. [57] state that fast quenching produce the best balance of strength and ductility. The study further states that the quench medium and interval has an effects on the effectiveness of quenching. They report that the properties of the A356 alloy, exposed to the T6 heat treatment and quenched in water, affected the sensitivity of the Ultimate Tensile Strength and Yield Strength more than ductility, when the water temperature surpassed 60-70°C. Detailed microscopy investigations on A356 alloy, reported by Zhang and Zheng [52], discovered that the β″-Mg_2Si precipitates' density decreased with slight increases in size with raised water quench temperature from 25°C to 60°C, and a rise in fine Si precipitates.

Quenching in air produce completely different precipitation feature. The material cools down slower, which causes an increase in the Si and Mg diffusion. Thus, a higher density of fine β″-Mg_2Si precipitates, but also an increase in rougher rod-like β′-Mg_2Si [52].

2.4.3. Ageing

The aim of aging is to acquire uniform distribution of the strengthening precipitates retained during quenching. This leads to a better homogenous material properties and improvements. Ageing can be done at room temperature called natural ageing or at an elevated temperature known as artificial ageing [41].

2.4.3.1. Natural ageing

At room temperature, the formation of Guinier-Preston (GP) zones occurs rapidly. These are groups of high concentrations of very small precipitates or solute atoms that are finely dispersed in a supersaturated metallic solid solution, because diffusion is limited at room temperature. The GP zones and the stress field around them hinder dislocation motion, resulting in an increase in strength [41]. Also, the hardening of Mg-containing phases happens

very quickly, and can be observed after about 1h. After about 100h no further increase in hardness occurs [58, 59]. The hardness is dependent on the Mg concentration in the alloy; a higher weight percentage (<0.7 wt.%) gives a greater hardness. Cu-containing phases has a slow response to hardness at room temperature, but minor additions of Mg cause hardness reaction to increase by natural ageing [60].

2.4.3.2. Artificial ageing

At an elevated temperature (150-210°C), particles can travel over greater spaces and the precipitates that develop are generally larger than the GP zones [41].

2.4.3.3. Precipitation sequence

The formation of the GP zones are the first process in the precipitation sequence, which is followed by the formation of the either coherent or semi-coherent metastable precipitates to the matrix. If these precipitates reach a critical size it may nucleate on the GP zones, or homogeneously in the matrix, or heterogeneously on dislocations or other lattice defects. The metastable precipitates grow on further ageing by diffusion of atoms from the supersaturated solid solution to the precipitates. As the supersaturation decreases, the precipitates continue to grow in accordance with Ostwald ripening [7].

The process is driven by a reduction in surface energy, so that the larger precipitates coarsen as the smaller ones dissolve. As the precipitates grow the coherency strain increases until interfacial bond strength is exceeded and the precipitates become non-coherent. Last to form in the precipitation sequence is the non-coherent equilibrium phase. The precipitation procedure does not necessarily follow the above sequence - it can also start at an intermediate stage, depending on the thermal history of the material (natural ageing, artificial ageing temperature, heating rate, etc.) [41].

2.4.3.4. Hardening mechanisms

The strength of an alloy is characterised by the precipitates capability to prevent dislocations from moving freely, which is dependent on the precipitates size and distribution and by the consistency with the matrix. The Friedel effect and the Orowan mechanism can by utilised to describe the interaction between the precipitates and dislocations. The Friedel effect occurs when the movement of dislocations shear small precipitates with intermediate hardness, see Figure 2.4 a. When the moving dislocations pass over bigger and harder precipitates, a bowing effect occurs, this is known as the Orowan mechanism, see Figure 2.4 b. The

precipitates strength is proportional to its size, on the condition that it is sheared by dislocation (Friedel effect). If the precipitates size is too large, that it prevents shearing to take place, thus causing the Orowan mechanism to occur, can lead to strength reduction, see Figure 2.4 c. The maximum strength is achieved when an equivalent chance for the dislocations to pass the precipitates by both shearing and bowing [41].

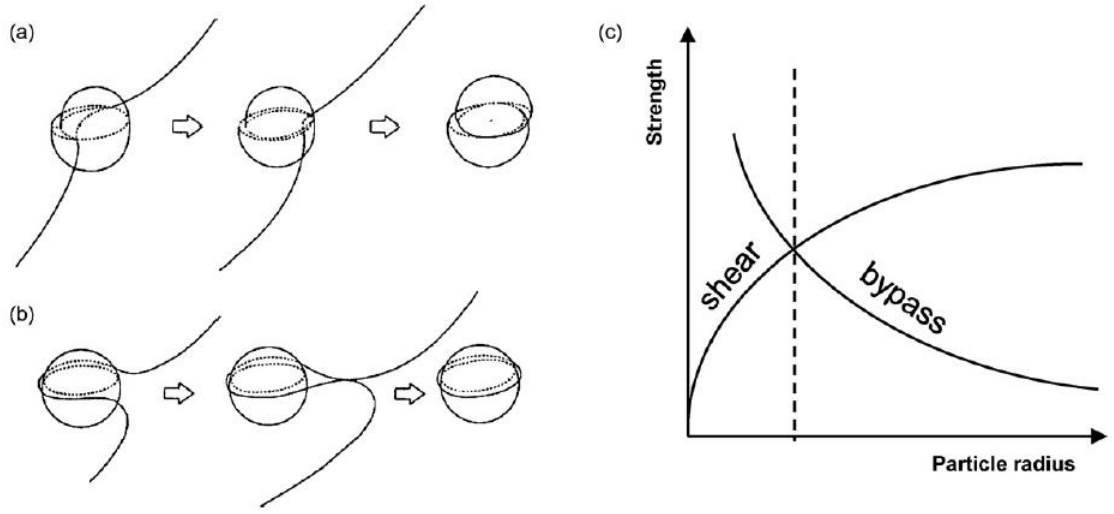

Figure 2.4: Dislocations pass precipitates by (a) shearing or (b) bypassing *[61]*. (c) Relationship between precipitate radius and strength of the particles to resist shearing or bypassing by dislocations *[11]*.

For Al-Si-Cu alloys, dense areas of Cu atoms with diameters between 3-5nm make up the GP zones formed at room temperature. Temperature increases above 100°C cause dissolution of these GP zones [62], which is replaces by θ″ phases (occasionally stated as GP2). Before the formation of the θ″ phase noticeable strength reductions can be observed. Extended ageing causes the θ″ phase to change into the metastable θ′, which is partially coherent with the matrix. The formation of the stable incoherent equilibrium phase θ (Al_2Cu) is formed during the last stage of ageing. Strength is proportional to the fraction of θ″ phase is present, thus the maximum strength accomplished with the highest number [62].

Al-Si-Cu alloys takes longer to obtain optimum hardness than for Al–Si–Mg and Al–Si–Cu–Mg alloys. Kang et al. [63] reported that hardness peak at 160°C for about 120h at and 15h at 200°C. An increase distribution of peak hardness are observed when the ageing time increase from 30h up to 120h [63, 64, 65, 66]. This is due to the Mg that greatly influence response to the ageing process [41].

2.4.4. Heat treatment modelling

Models can assist in the design of new alloys that requires to meet a certain criteria or specification and help in gaining knowledge about the microstructural influence on the properties of alloys [7]. Shercliff and Ashby [67] developed the first model that coupled the yield strength to the microstructural evolution during artificial ageing. It mathematically took in to consideration the process variables (e.g. alloy composition, heat treatment temperature and time), and how it affected the mechanical properties (e.g. yield strength, hardness), with respect to the physical principles (e.g. thermodynamics, kinetics of precipitation, strengthening mechanisms etc.).

2.4.4.1. Solution heat treatment modelling

According to Sjölander and Seifeddine [8], one can model the solution heat treatment based on diffusion, whereby assuming spherical particles with a spherical diffusion field produce experimental results with good outcomes. They state that by making use of a measured distance between the Al_2Cu phases to calculate the diffusion field gives a slower dissolution and homogenisation rate compared to the experimental results. Decreasing the interparticle distance, so that it includes only the α-Al phase, and assuming a high diffusion coefficient in the Si eutectic, gives good agreement with the experimental results.

The basic model (Figure 2.5) is similar to the 1-D models at the scale of the dendrite arms. The initial condition reflects the segregation profile produced by solidification, and in particular the volume fraction of the primary α-phase given by g_α^p. The fraction of eutectic formed is thus $g_{eut} = 1 - g_\alpha^p$. The heat treatment takes place at a temperature between the solvus temperature for the alloy and the eutectic temperature, shown as the dashed line in Figure 2.5a. It is assumed that the eutectic region is at local equilibrium, which implies that the composition of the α-phase at the eutectic region is given by the solvus value C_α and the composition of the α-phase in the eutectic region is given by C_β. The volume fraction of β-phase is designated as g_β, and the volume fraction of α-phase in the $\alpha + \beta$ region thus becomes $1 - g_\alpha^p - g_\beta$. The composition of the α-phase in the eutectic is assumed to remain constant, even as the β-phase dissolves. This is a reasonable assumption when g_β is small. [31]

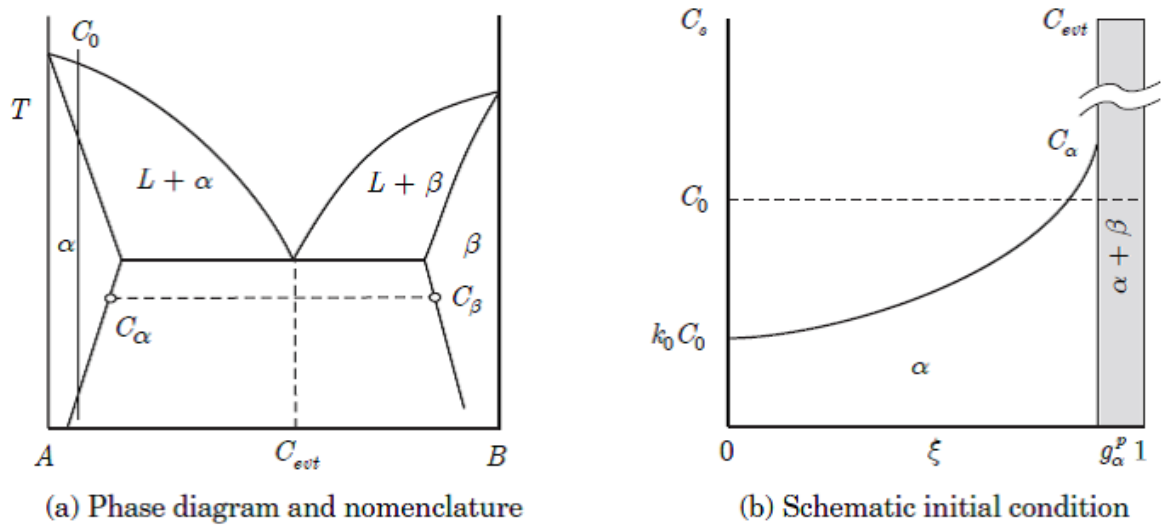

(a) Phase diagram and nomenclature (b) Schematic initial condition

Figure 2.5: A schematic view of (a) the phase diagram and (b) initial condition for solution treatment analysis *[31]*

The governing equation and boundary conditions for this problem under the stated assumptions are

$$\frac{\partial C_{s,i}}{\partial \tau} = \frac{4D_{s,i}t_f}{\lambda_2^2}\frac{\partial^2 C_{s,i}}{\partial \xi^2} \qquad 0 \le \xi \le g_\alpha \qquad (14)$$

$$\frac{\partial C_{s,i}}{\partial \tau} = 0 \qquad \xi = 0 \qquad (15)$$

$$C_{s,i} = C_\alpha \qquad \xi = g_\alpha \qquad (16)$$

The solution can be written in as a Fourier cosine series

$$C_{s,i}(\xi,\tau) = C_\alpha + \sum_{m=1}^{\infty} A_m \cos\left(\frac{(2m-1)\pi\xi}{2g_\alpha}\right) e^{-(2m-1)^2\pi^2\tau/2g_\alpha^2} \qquad (17)$$

An initial condition is required to evaluate the coefficient A_m. From experience, the initial condition quickly disappears, thus it is quite reasonable to choose an approximate initial condition of the form

$$C_{s,i}(\xi,\tau) \approx C_\alpha + A_0 \cos\left(\frac{\pi\xi}{2g_\alpha}\right). \qquad (18)$$

Note that, with this simple form, it is not possible to choose a single constant A_0 that satisfies the boundary condition on $C_{s,i}$ at $\xi = 0$ and $\xi = g_\alpha$, and to enforce a total solute balance all at the same time. It will be demonstrated, however, that the exact choice of A_0 is unimportant for the analysis, and thus choose A_0 to ensure that the total solute content is equal to C_0. With this choice of the initial condition, only the leading term in the series has a non-zero coefficient, and the solution is given by

$$C_{s,i}(\xi,\tau) = C_\alpha + A_0 \cos\left(\frac{\pi\xi}{2g_\alpha}\right) e^{-\pi^2\tau/4g_\alpha^2} \tag{19}$$

Next, a solute balance over the domain at $\tau = 0$ is performed:

$$\int_0^{g_\alpha} C_{s,i}(\xi,0)\,\mathrm{d}\xi + C_\alpha\left(1 - g_\alpha^p - g_\beta^0\right) + g_\beta^0 C_\beta = C_{0,i} \tag{20}$$

where g_β^0 is the fraction of β-phase at $\tau = 0$. Substituting Equation (14) into the above and after manipulation,

$$\int_0^{g_\alpha} A_0 \cos\left(\frac{\pi\xi}{2g_\alpha}\right)\mathrm{d}\xi = -(C_\alpha - C_{0,i}) - (C_\beta - C_\alpha)\, g_\beta^0 \quad . \tag{21}$$

Computing a similar solute balance at time τ yields

$$\left[\int_0^{g_\alpha} A_0 \cos\left(\frac{\pi\xi}{2g_\alpha}\right)\mathrm{d}\xi\right] e^{-\pi^2\tau/4g_\alpha^2} = -(C_\alpha - C_{0,i}) - (C_\beta - C_\alpha)\, g_\beta^0. \tag{22}$$

Dividing Equation (18) by Equation (17) provides a relation between the volume fraction of β-phase and time

$$\frac{g_\beta + (C_\alpha - C_{0,i})/(C_\beta - C_\alpha)}{g_\beta^0 + (C_\alpha - C_{0,i})/(C_\beta - C_\alpha)} = e^{-\pi^2\tau/4g_\alpha^2} \quad . \tag{23}$$

Note that Equation (19) takes a particularly simple form when the heat treatment is done at the solvus temperature of the alloy, where $C_\alpha = C_{0,i}$. Thus, simplifying to the Scheil equation.

2.5. Metal Casting Software

MAGMASOFT employs the finite difference method to solve the heat and mass transfer on a rectangular grid. It is a useful tool for simulating molten metal flow. It is a comprehensive simulation tool featuring capabilities that show mould filling, solidification, mechanical properties, thermal stresses and distortions, both for ferrous and non-ferrous alloys. It is widely used in the metal casting industry, particularly in foundry applications, for modelling the molten metal flow and solidification in dies [68].

2.5.1. Finite Difference Method

The goal of discretisation is to find a set of cut points to partition the range into a small number of intervals that have good class coherence, which is usually measured by an evaluation function. In addition to the maximisation of interdependence between class labels and attribute values; an ideal discretisation method should have a secondary goal to minimise the number of intervals without significant loss of class attribute mutual dependence [69].

The finite difference method, also known as the Euler method, is a numerical technique for solving differential equations. Numerical techniques only find approximate solutions, but are much easier to solve than techniques for finding exact solutions or formulae for exact solutions [70, 71]. It involves replacing the derivative in the differential equation with algebraic equations to get approximated solutions. The domain is partitioned in space and time, and approximations of the solution are computed at the space or time points. The error between the numerical solution and the exact solution is determined by the error that is committed by going from a differential operator to an algebraic operator. This error is called the discretisation error or truncation error [72]. Thus, an awareness of the error is necessary in order to set appropriate discretisation intervals.

By definition of a derivative [71, 73]:

$$f'(x) = \lim_{\Delta x \to 0} \frac{f(x+\Delta x) - f(x)}{\Delta x} = \lim_{\Delta x \to 0} \frac{f(x) - f(x-\Delta x)}{\Delta x} = \lim_{\Delta x \to 0} \frac{f(x+\Delta x) - f(x-\Delta x)}{2\Delta x} \tag{24}$$

and Taylor series expansion:

$$f(x+\Delta x) = f(x) + \Delta x\, f'(x) + \frac{\Delta x^2}{2!} f''(x) + \frac{\Delta x^3}{3!} f^{(3)}(x) + \cdots, \tag{25}$$

or

$$f(x-\Delta x) = f(x) - \Delta x\, f'(x) + \frac{\Delta x^2}{2!} f''(x) - \frac{\Delta x^3}{3!} f^{(3)}(x) + \cdots, \tag{26}$$

Rearranging equation (25) gives an approximation for equation (24), known as the forward difference approximation:

$$f'(x) \approx \frac{f(x+\Delta x) - f(x)}{\Delta x} = f'(x) + \mathcal{O}(\Delta x) \tag{27}$$

where $\mathcal{O}(\Delta x) = \frac{\Delta x}{2!} f''(x) - \frac{\Delta x^2}{3!} f^{(3)}(x) + \cdots,$ known as the truncation error, and means 'of order Δx', which leads the expression to read that the derivative of f at x, and has an error of size Δx; the approximation is said to be first order accurate [70, 73].

Rearranging Eq. (26) gives an approximation for Eq. (24), known as the backward difference approximation:

$$f'(x) \approx \frac{f(x) - f(x-\Delta x)}{\Delta x} = f'(x) + \mathcal{O}(\Delta x) \quad , \tag{28}$$

which is also first order accurate, since the error is of order Δx. Subtracting Eq. (26) from Eq. (25) gives the centred difference approximation:

$$f'(x) \approx \frac{f(x+\Delta x) - f(x-\Delta x)}{2\Delta x} = f'(x) + \mathcal{O}(\Delta x)^2 \tag{29}$$

which is second order accurate since the error is of order $(\Delta x)^2$.

Knowing that the order is very important, as the higher the order the more accurate the solution, the centred difference scheme therefore gives a better approximation [72, 73]. However the higher order schemes need more algebraic operations, and hence requires greater computational time.

From Mochnacki and Suchy [70], the differential approximation for the second order derivative is given by:

$$f''(x) \approx \frac{f(x+\Delta x) - 2f(x) + f(x-\Delta x)}{\Delta x^2} = f''(x) + \mathcal{O}(\Delta x)^2 \tag{30}$$

After applying FDM, the left hand side of equation (14) can be rewritten as a set of algebraic equation:

$$\frac{C_{i+1}^{f} - C_{i}^{f}}{\Delta \tau} = \frac{4D_{s,i}t_f}{\lambda_2^2}\left(\frac{C_{i+1}^{f} - 2C_{i}^{f} + C_{i-1}^{f}}{(\Delta \xi)^2}\right) \tag{31}$$

where $C_i^f = C(t_f, x_i)$ is a given element concentration at i*th* point of discrete grid at f*th* layer of time.

Chapter 3. Experimental Procedure and Analysis

3.1. Objective

The aim of the empirical investigation is to compare the simulated solutions with the actual experimental results. This will occur by comparing the microstructure of the samples from both the as-cast and heat treated castings. The goal will be to observe the evolution or changes in the intermetallic phases as mentioned in the literature review. Since the heat treatment process is being conducted at a higher temperature than prescribed by literature, there might be the possibility to observe the dissolution of hard to dissolved phases. This can have beneficial outcomes, as these phases can aid as improvement to the mechanical properties of the alloy. If this can be achieved, it can assist in understanding the alloy's behavior, whereby conclusions can be drawn for future studies and improvement.

3.2. Computer Simulation and Setup

MAGMASOFT®, is a powerful software for simulating and to provide better knowledge of mould filling, solidification and cooling, and allows for measureable expectation of mechanical properties, thermal stresses and distortions of the final castings.

The newest release, MAGMA5, contains additional modules, such as MAGMAnonferrous, which is a material-specific module that allows for predicting the microstructures and properties of nonferrous alloys. There is also the MAGMA HT thermal and MAGMAstress modules that allow simulation of heat treatment and the deformation of the part (internal stress field calculation) after casting respectively.

The simulation also produces results for the prediction of possible microstructural phases for the casting from the MAGMAnonferrous**,** with the Micro Modelling Aluminium add-on. This is for aluminium alloys with recommended ranges for Si (6.5-12.5wt%); Fe (0-0.6wt%); Mg (0-0.6wt%); Cu (0-3.5wt%); Mn (0-0.4wt%); other (≤2wt%). It is important that composition is set within the ranges to avoid possible errors.

It also simulates and produces results for the material properties, and even though heat treatment schedules is user-defined and the setup is manually entered, the results obtained for the microstructural phases is based on a standard T6 heat treatment process with a solution heat treatment schedule of 6h at 495°C for composition containing 1-3wt% Cu, or 6h at 525°C when containing Mg. This is followed by water quenched at 50°C, natural aging for

24h, and finally artificial aging for 8h at 175°C. The MAGMA HT thermal results are only thermal profiles and stresses bases on the temperature and cooling rates.

3.2.1. Computer Aided Design

The design of the experimental casting is a basic square (figure 3.1) with a gating system to reduce turbulent flow. This is to minimize surface expose to air, due to aluminium's ability to quickly form oxide layers, which can be detrimental to the materials properties when solidified. Three different section sizes (10, 12.5, 15mm) were simulated to identify and compare the cooling rates with respect to the thicknesses.

The computer aided drawings were generated using SOLIDWORKS**,** saved as an STL file and imported into MAGMASOFT®.

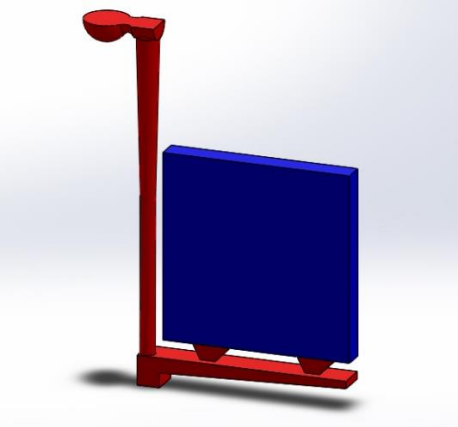

Figure 3.1: 3D model of a casting (blue) including gating system (red).

3.3. Mould Preparation

The preparation for the mould commenced with first 3D printing the shapes (figure 3.2) of the different gating system components using a UP! 3D printer and acrylonitrile butadiene styrene (ABS) as the model material.

Figure 3.2: 3D print of gating system

Green sand was utilised for the mould (figure 3.3) with thermocouples placed inside the mould, at the centre, and one within the casting cavity, to measure the temperature during the casting process (see figure 3.4).

Figure 3.3: Sand mould.

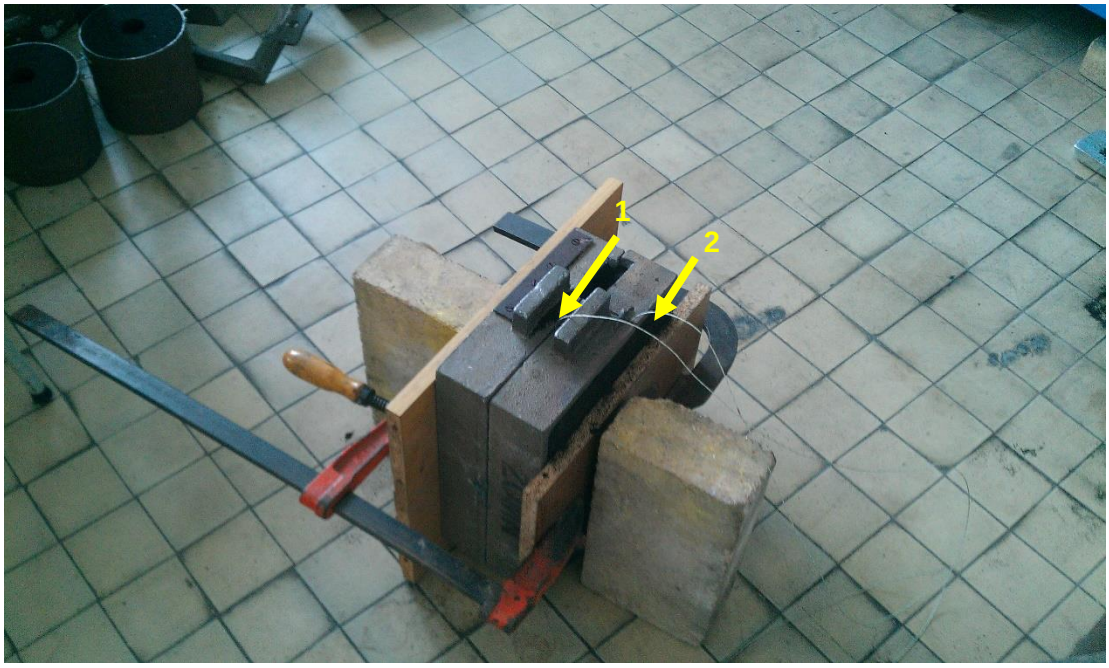

Figure 3.4: Assembled mould with thermocouples (1 – casting cavity; 2 – centre of inside mould)

3.4. Alloy, Equipment and Casting

The aluminium alloy, AK-64, is a name allocated to the alloy grade in Poland (PN-76/H-88027), and is similar to the Aluminum Association (AA) 319.0. The difference in composition is captured in Table 3.1. It was supplied as ingots from the Institute of Non-Ferrous Metals, Light Metals Division in Skawina, Poland.

The ingots were melted in an induction furnace (Czylok PT 40/1300), at a temperature of 750°C, and after achieving a complete molten state, the melt was poured into the mould (figure 3.4). An Agilent 34970A Data Acquisition Switch unit with K-type thermocouples was used to register the temperature change during cooling.

After cooling to room temperature, the castings were removed from the mould and cleaned, to remove any visible sand burn and/or additional unwanted material (figure 3.5). Six plates of three different thicknesses were cast- two plates of each thickness: 10 mm, 12.5 mm and 15 mm.

Table 3.1: Element compositional comparison

Element	**AK 64 ingot [1] wt%**	**AK 64 (PN-76/H-88027), wt%**			**A319.0** [2]**, wt%**
Silicon	6.07	5.0-7.0			5.5-6.5
Copper	3.75	3.0-5.0			3.0-4.0
Iron	0.59	**Lp**	**Lk**	**Lc**	1.0 max
		1.0	1.2	1.4	
Manganese	0.45	0.3-0.6			0.5 max
Magnesium	0.23	0.5			0.1 max
Zinc	0.11	2			1.0 max
Titanium	0.05	0.15			0.25 max
Nickel	-	0.5			0.35 max
Other (impurities)		4.0	4.2	4.4	0.5

Figure 3.5: Casting (including gating system).

[1] Composition was measured in supplier's laboratory, and certificate issued.

3.5. Heat Treatment

The heat treatment schedule that was selected for the experiment was the same as the one used in the MAGMASOFT® heat treatment module. This was to have a correlation and to allow comparison between the numerical and experimental results.

It follows a T6 heat treatment process with the following steps:

1. Solution heat treatment for 6 hours at 525°C due to the magnesium content;
2. Water quenched at 50°C;
3. Artificial ageing at 175°C for a duration of 8 hours;
4. And then the samples is allowed to cool down within the heat treatment furnace to room temperature

The heat treatment process was conducted using a Czylok PT 12/1300 induction furnace.

3.6. Metallography

3.6.1. Specimen preparation

Specimens were sectioned from the casting according to the depiction in Figure 3.7, and was carried out mechanically by means of sawing. The aim was to obtain specimens as close as possible to the thermocouple, relate to the thermal history, and to avoid the porosity as predicted in MAGMASOFT®.

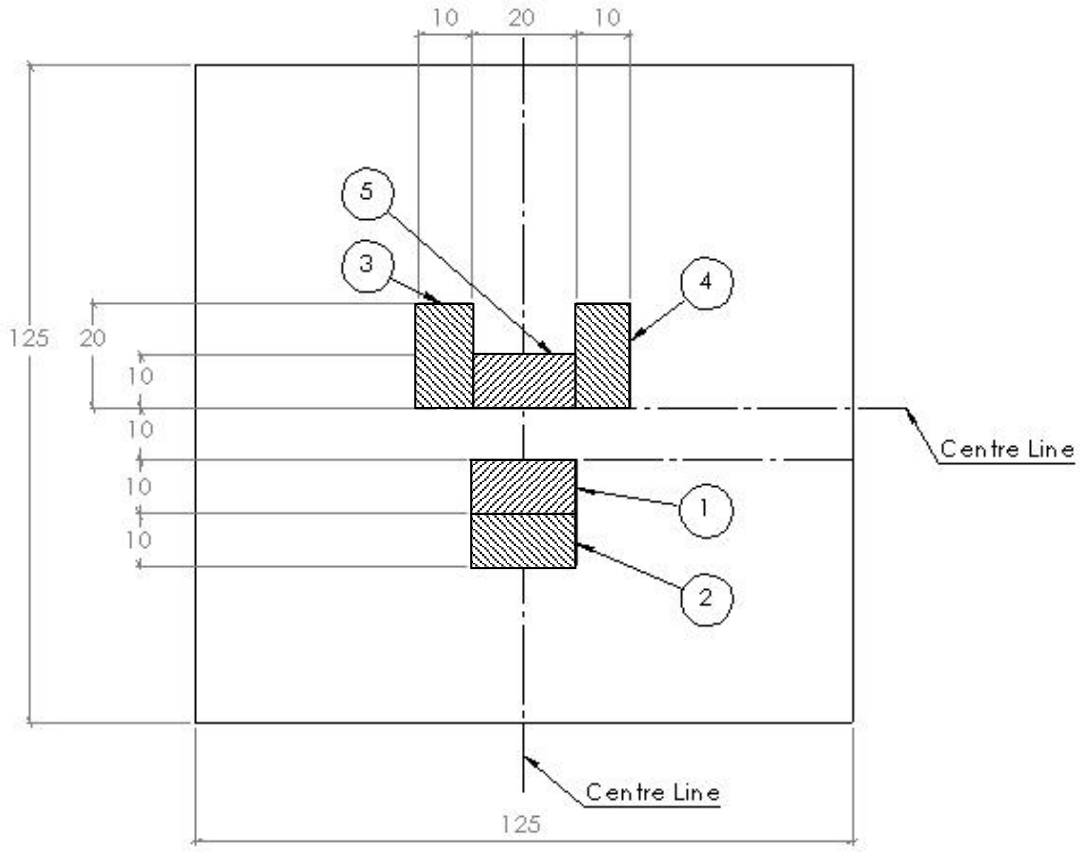

Figure 3.6: Indication of obtaining samples from casting. Numbers 1 to 5 indicate sample numbers.

The specimens were cold mounted in an acrylic resin, making use of the VersoCit-2 Kit. After the specimens were cured, grinding and polishing was carried out in the following order:

1. Wet grinding with water on a silicon carbide (SiC) foil with grain size 46µm, to remove the resin layer and for surface levelling;
2. Wet grinding with water on a SiC foil with grain size 22µm, to remove porosity from the upper surface;
3. Wet grinding with water on a SiC foil with grain size 15µm, to remove scratches;
4. Wet grinding with water on a SiC foil with grain size 5µm to remove scratches;
5. Fine grinding with water-based diamond suspension fluid (DiaPro) on a MD-Largo disk with grain size 9 µm for material removal;
6. Polishing on MD-Mol disk with grain size 3µm with water-based diamond suspension fluid (DiaPro); and
7. Final polishing on MD-Chem (porous neoprene) with OP-U suspension (colloidal silica suspension) with grain size 1µm.

After polishing of the specimens, etching is required to reveal the microstructure and for the identification of intermetallic phases. The Keller etchant was utilised to reveal the microstructures and phases. Specimens were submerged for 60 and 90 seconds.

3.6.2. Microstructural Analysis

Six specimens from each of the castings were send for X-ray diffraction (XRD) for the identification of the primary, eutectic and intermetallic phases. Optical Microscopy was used for the analysis of the specimens that were etched. An additional Scanning Electron Microscopy (SEM) analysis was conducted to precisely identify phases and compositions that could not be observed through the other aforementioned techniques.

Chapter 4. Results and Discussion

4.1. Simulation Results

It was observed from the MAGMASOFT® results that porosity occurred at almost the same regions in all three casting samples (Figures 4.1 - 4.3), with minor differences in the percentage or degree of occurrence. This can be attributed to the cooling (solidification) rate (Figures 4.4 - 4.6), as throughout literature it is well known that faster cooling or solidification of a casting affects the microstructure, causing smaller pores or less porosity to appear. This is also a function of the section thickness, as thicker sizes have more mass to solidify and therefore cools down slower. It can also be justified by the SDAS (Figures 4.7-4.9), that increases with slower cooling rates. The solidification time (liquidus to solidus) and cooling rate for the 10mm, 12.5mm and 15mm castings are about 155s, 185s and 218s, and 15.3°*C/s*, 9.83°*C/s* and 4.967°*C/s,* respectively as calculated by MAGMASOFT®.

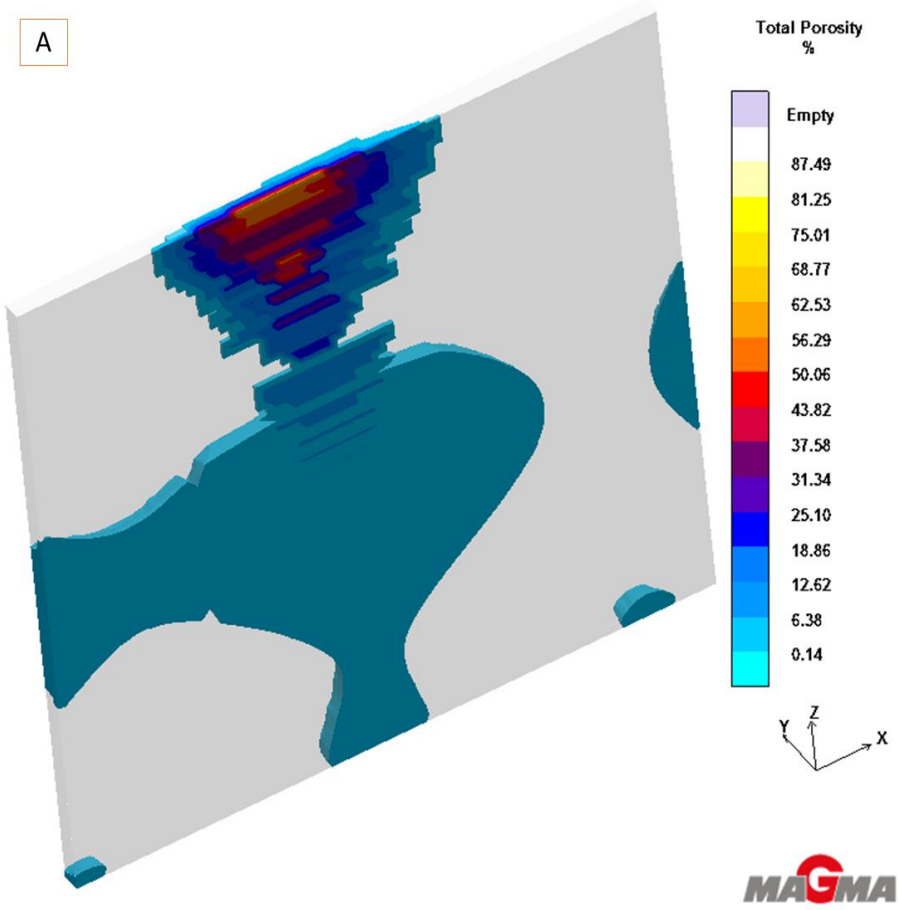

Figure 4.1: Total porosity in the casting, 10mm thickness

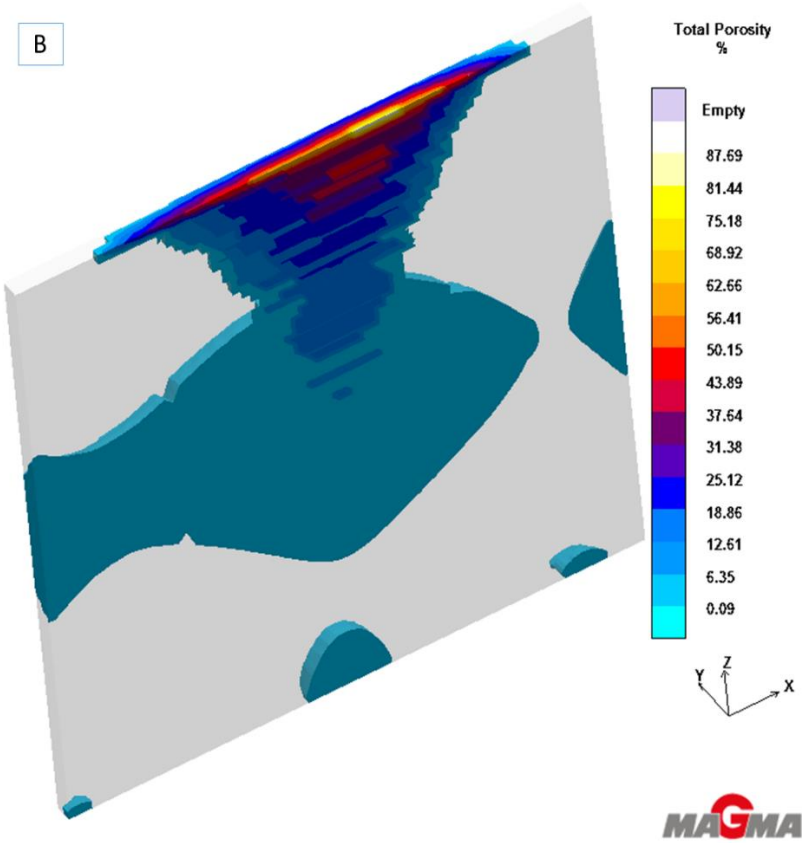

Figure 4.2: Total porosity in the casting, 12.5mm thickness

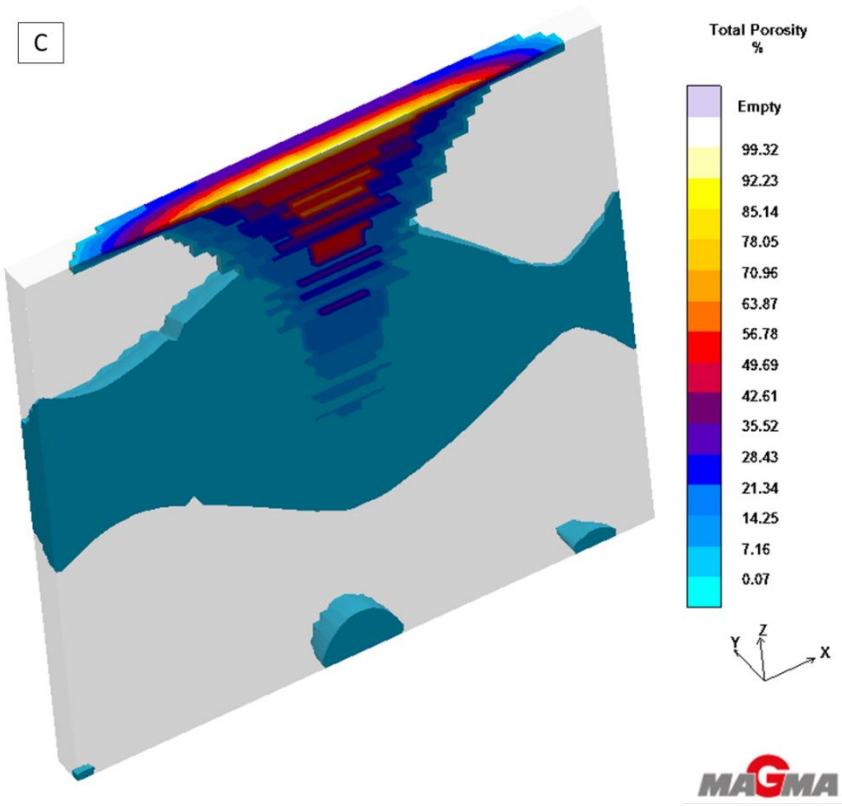

Figure 4.3: Total porosity in the casting, 15mm thickness

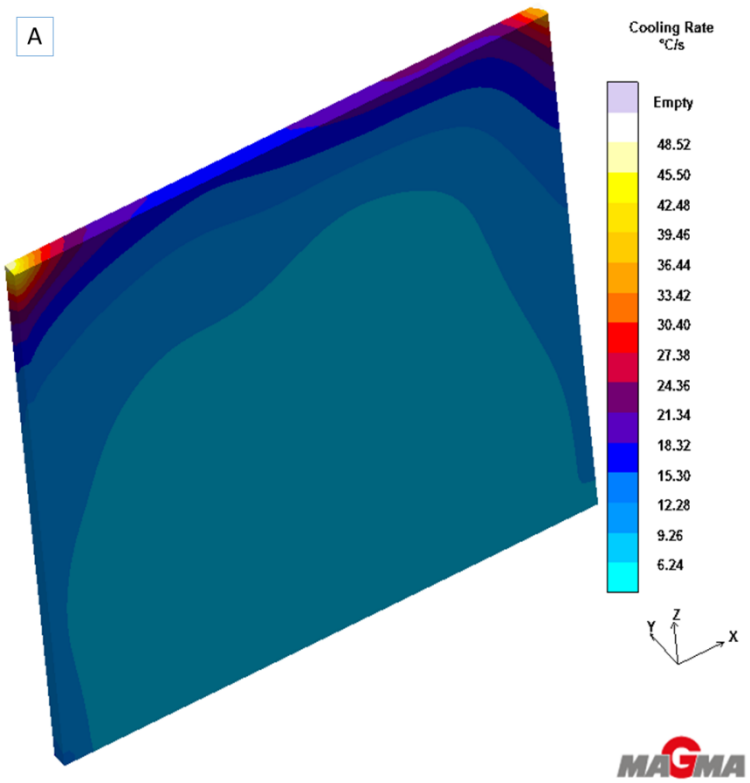

Figure 4.4: Cooling rate (°C/s) in the casting for 10mm thickness

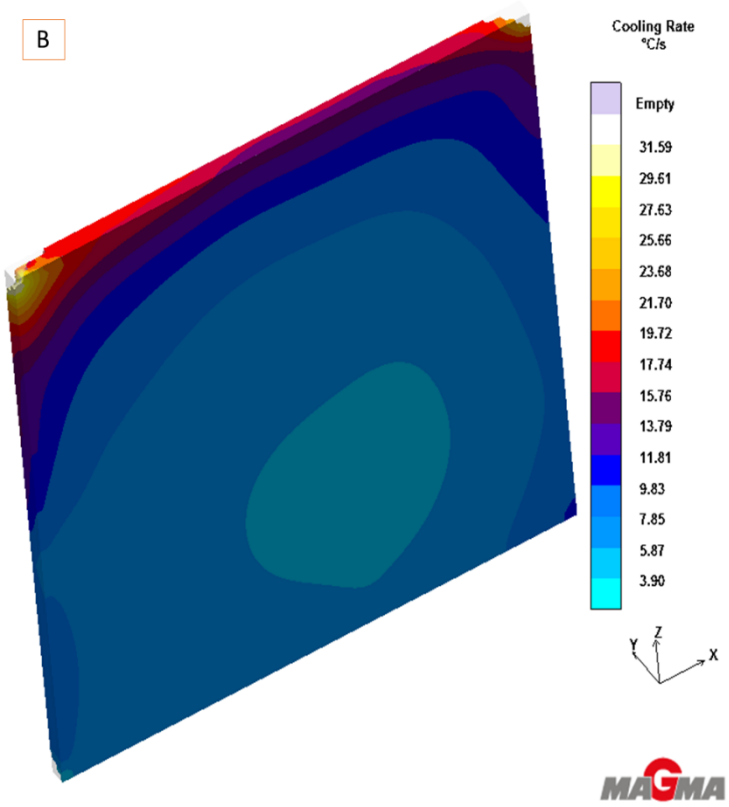

Figure 4.5: Cooling rate (°C/s) in the casting for 12.5mm thickness

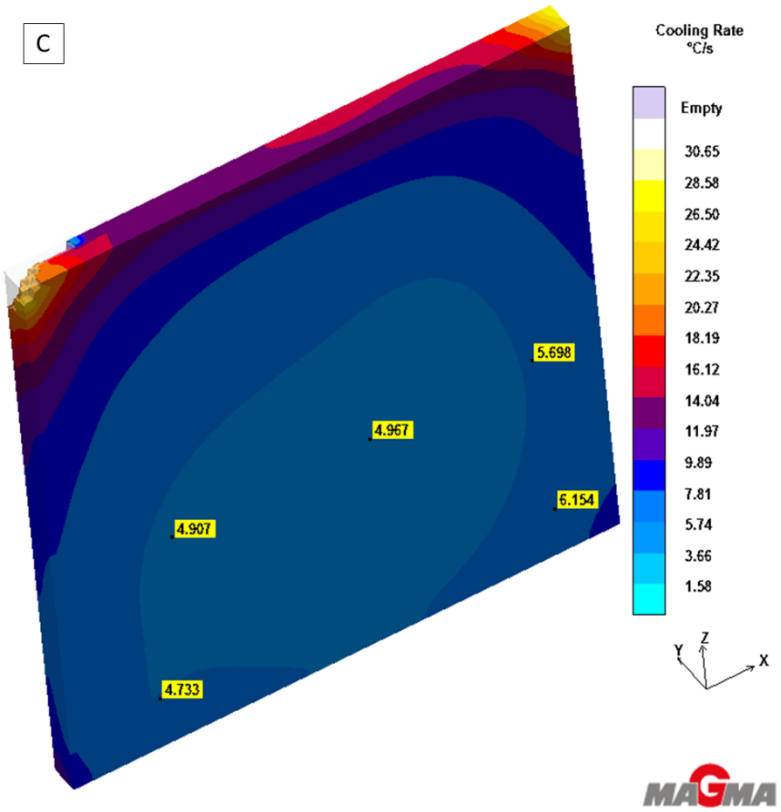

Figure 4.6: Cooling rate (°C/s) in the casting for 15mm thickness

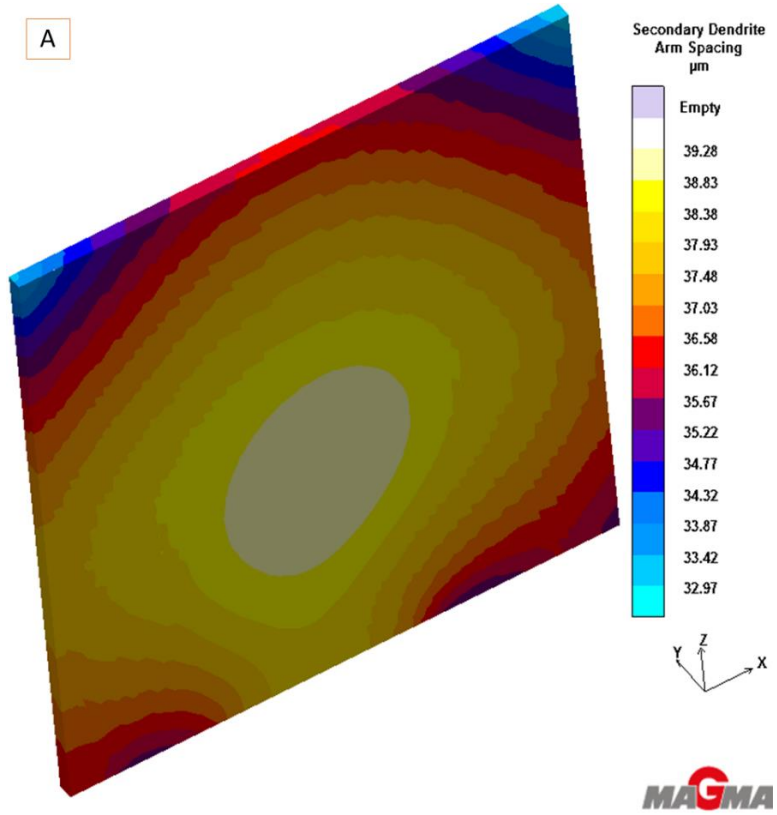

Figure 4.7: Secondary Dendrite Arm Spacing (SDAS) in the casting for 10mm thickness

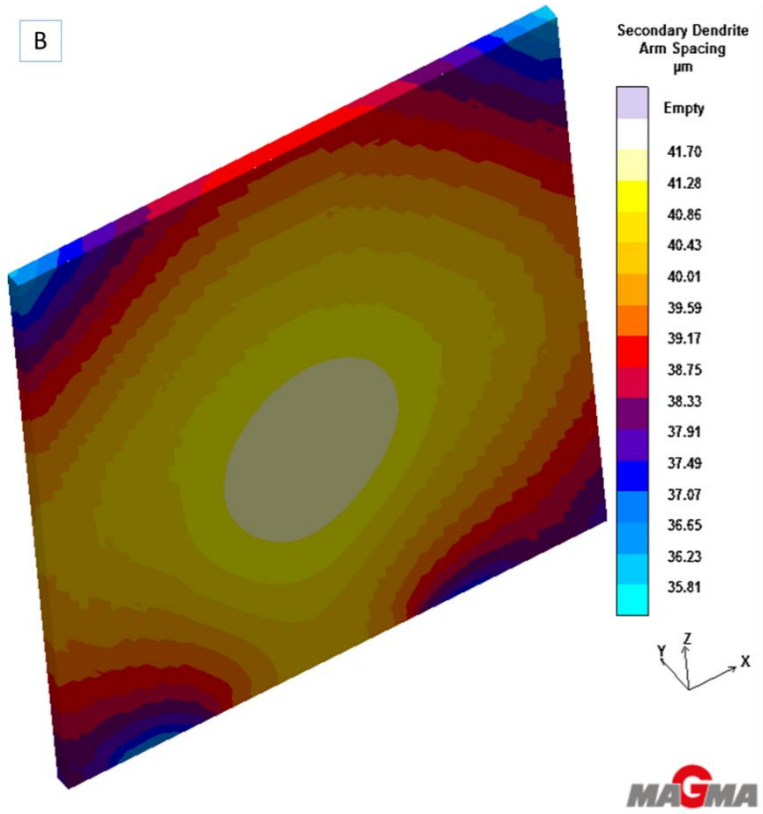

Figure 4.8: Secondary Dendrite Arm Spacing (SDAS) in the casting for 12.5mm thickness

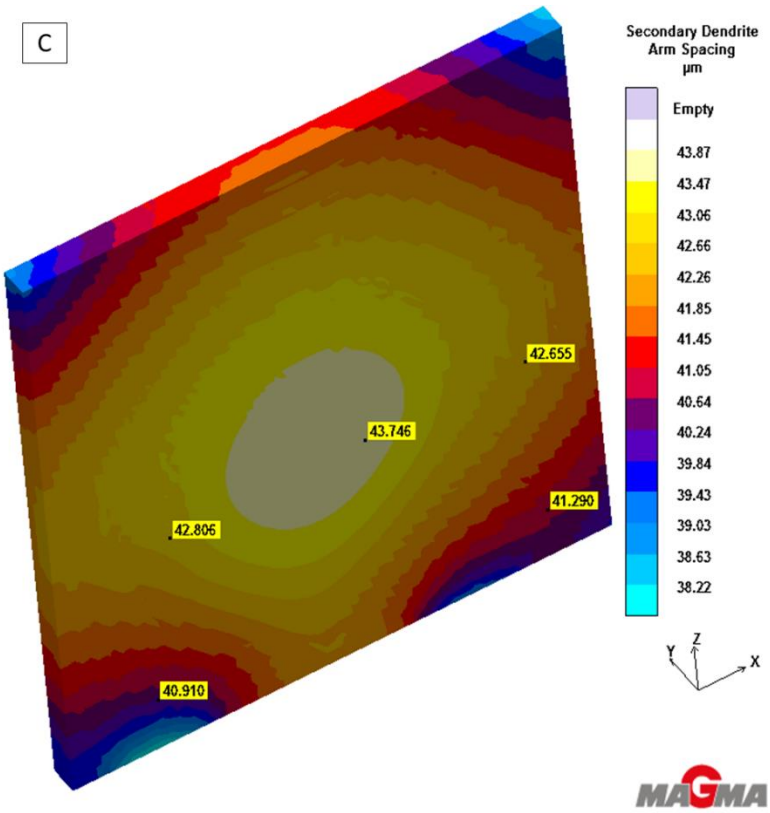

Figure 4.9: Secondary Dendrite Arm Spacing (SDAS) in the casting for 15mm thickness

The projected fractions of phases for the Al_2Cu phase for all sections was about 4.3% (figures 4.10-4.12), concentrated higher in the centre, and increasing with section thickness.

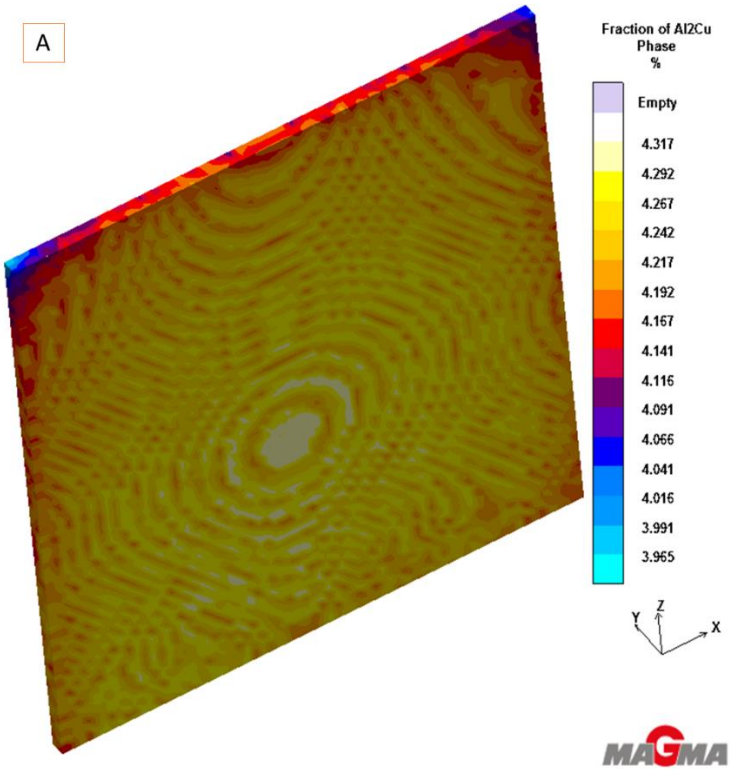

Figure 4.10: Fraction of Al_2Cu phase in the casting for section thickness 10mm

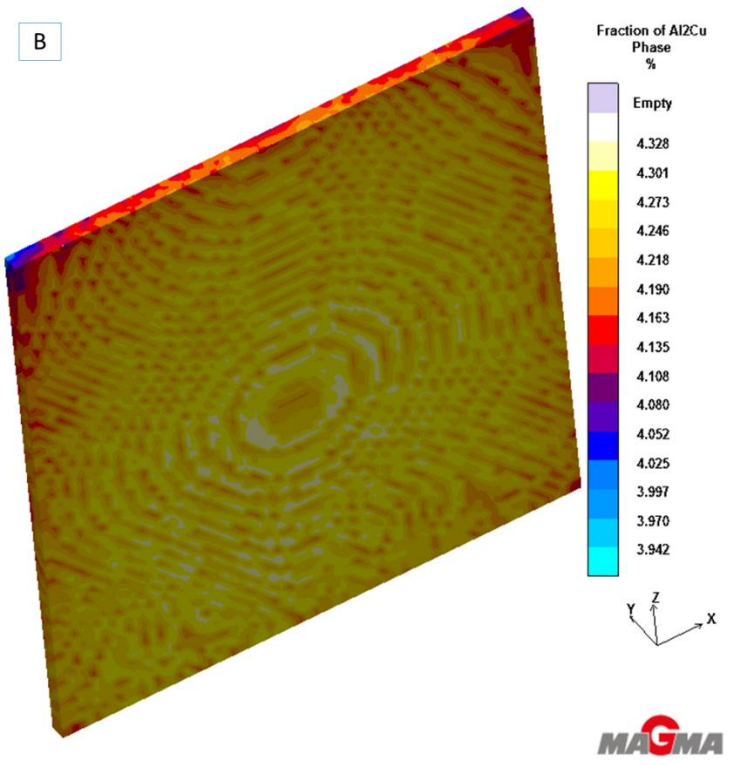

Figure 4.11: Fraction of Al_2Cu phase in the casting for section thickness 12.5mm

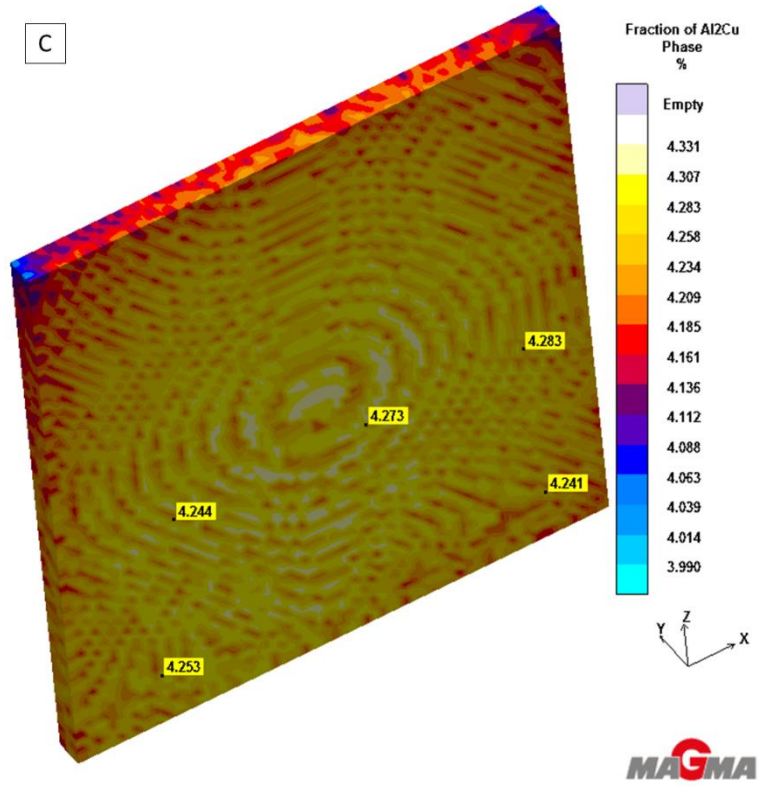

Figure 4.12: Fraction of Al_2Cu phase in the casting for section thickness 15mm

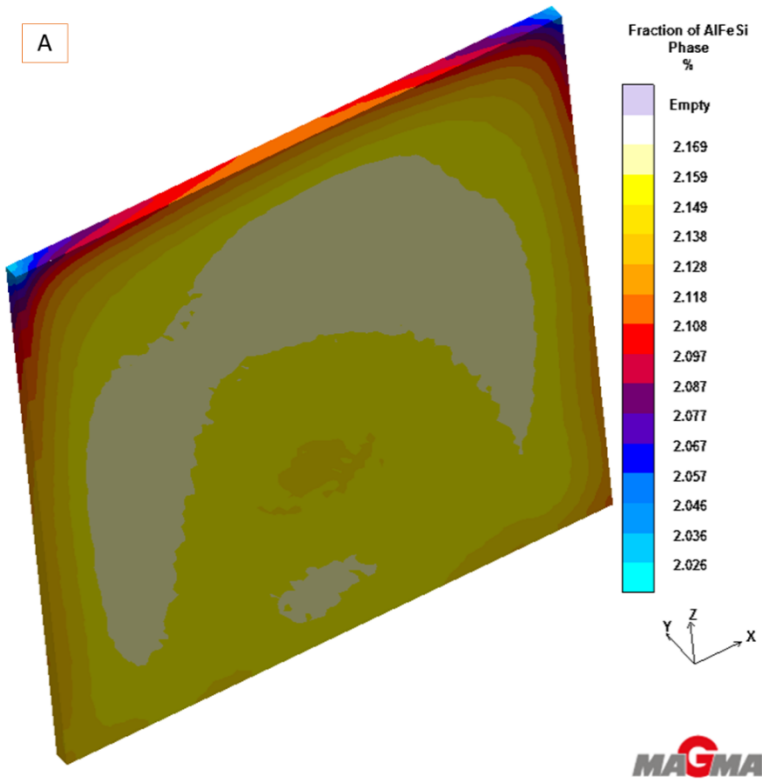

Figure 4.13: Fraction of AlFeSi in the casting for section thickness 10mm

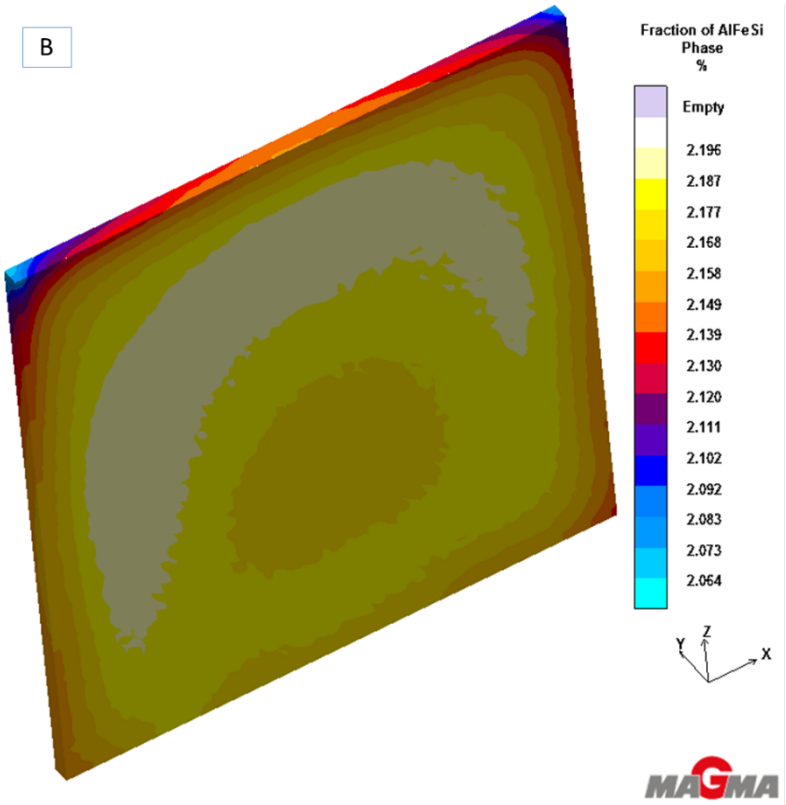

Figure 4.14: Fraction of AlFeSi in the casting for section thickness 12.5mm

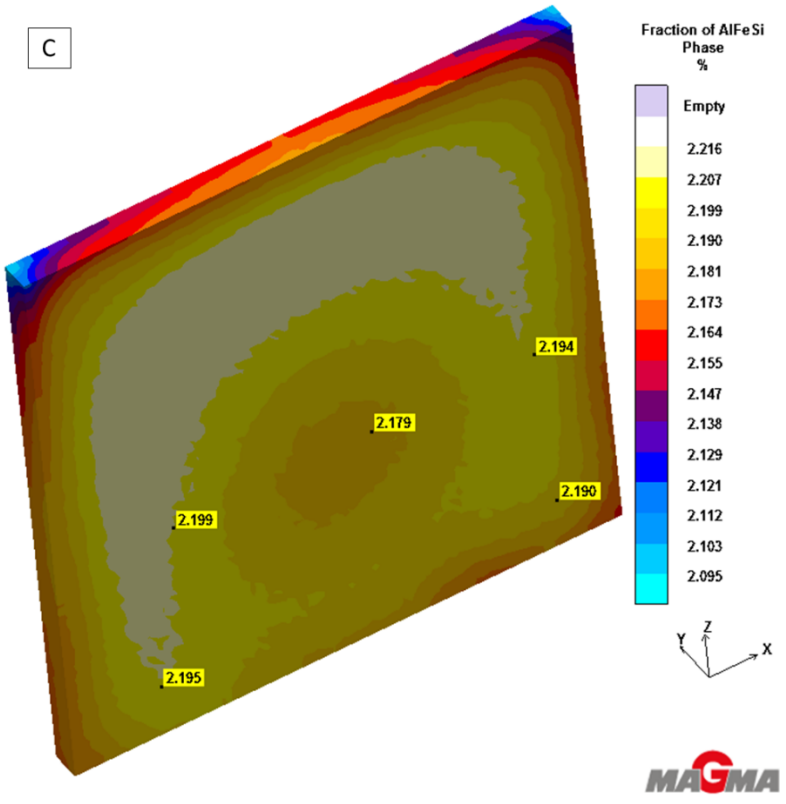

Figure 4.15: Fraction of AlFeSi in the casting for section thickness 15mm

The fractions of AlFeSi phases for all sections was just over 2% (figures 4.13-4.15), with higher concentrations around the centre, and increasing with section thickness. The reason for the concentration being higher around the centre can be ascribed to the higher melting temperature of Fe and Si, therefore solidifying first.

The results also produced the dispersion of other phases that are present within the casting, namely the eutectic, primary and Mg_2Si phases, but the first two are of little relevance, and the latter just a forecast due to the small composition, and could even be identified during the metallographic analysis, which will be discussed later.

The next set of results is the probable material properties, based upon the as-cast and T6 heat treatment, with respect to the elongation, tensile and yield strength (Figures 4.16 - 4.24). As can be observed, the elongation is the same for sections in the as-cast state, but decrease with heat treatment as the material becomes slightly harder and less ductile. The strengths increase as expected with heat treatment, but is below 250MPa as stated in literature.

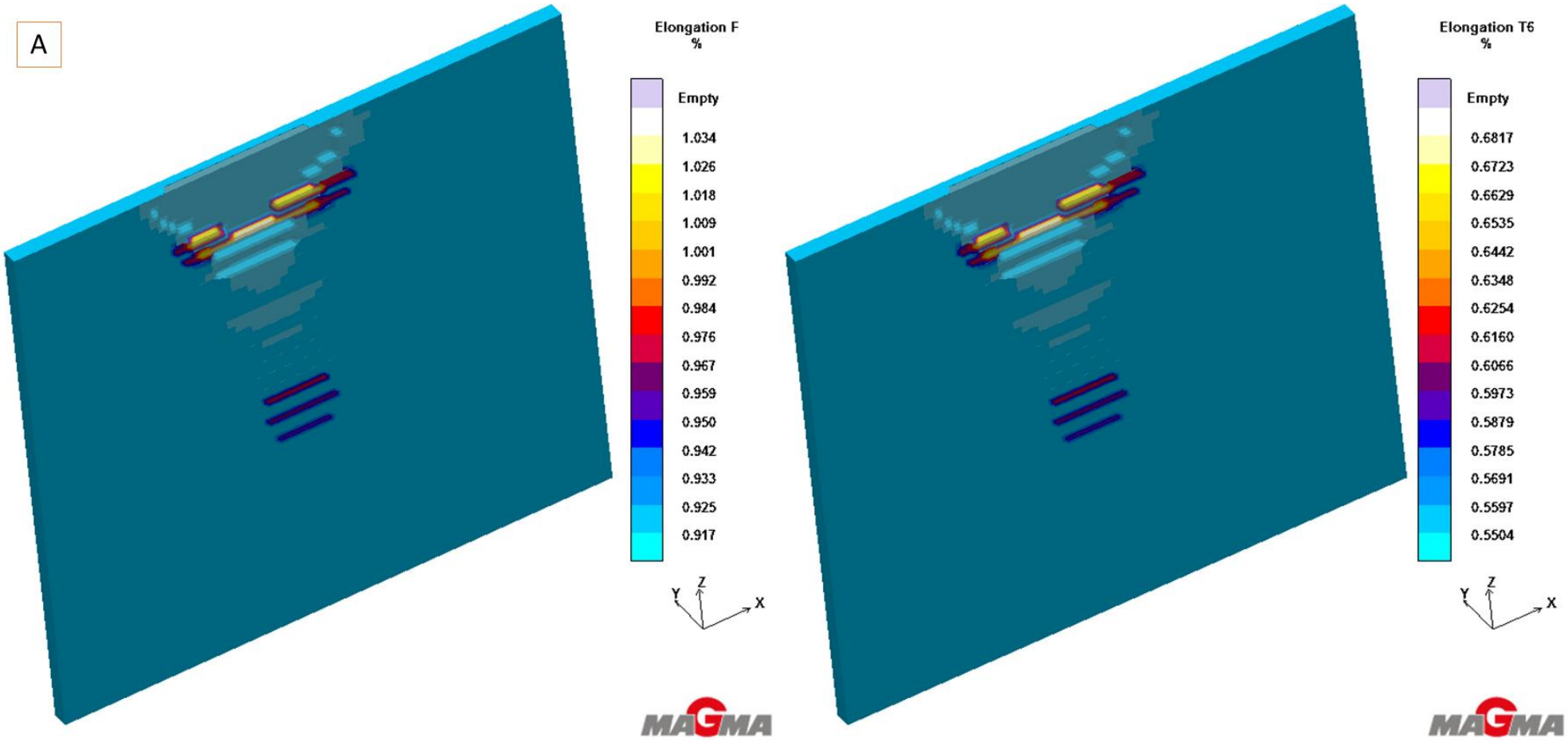

Figure 4.16: Elongation of the As-cast (F) and T6 heat treated castings for section thickness 10mm

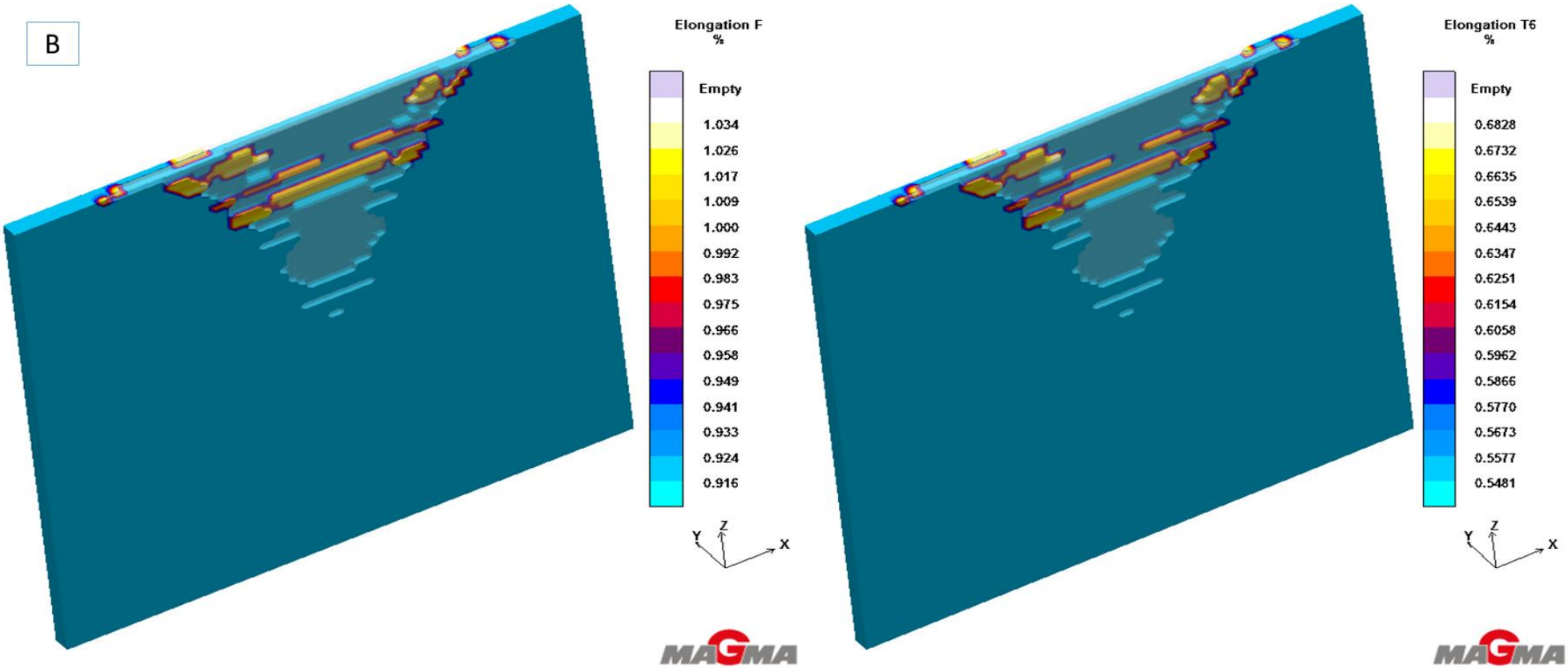

Figure 4.17: Elongation of the As-cast (F) and T6 heat treated castings for section thickness 12.5mm

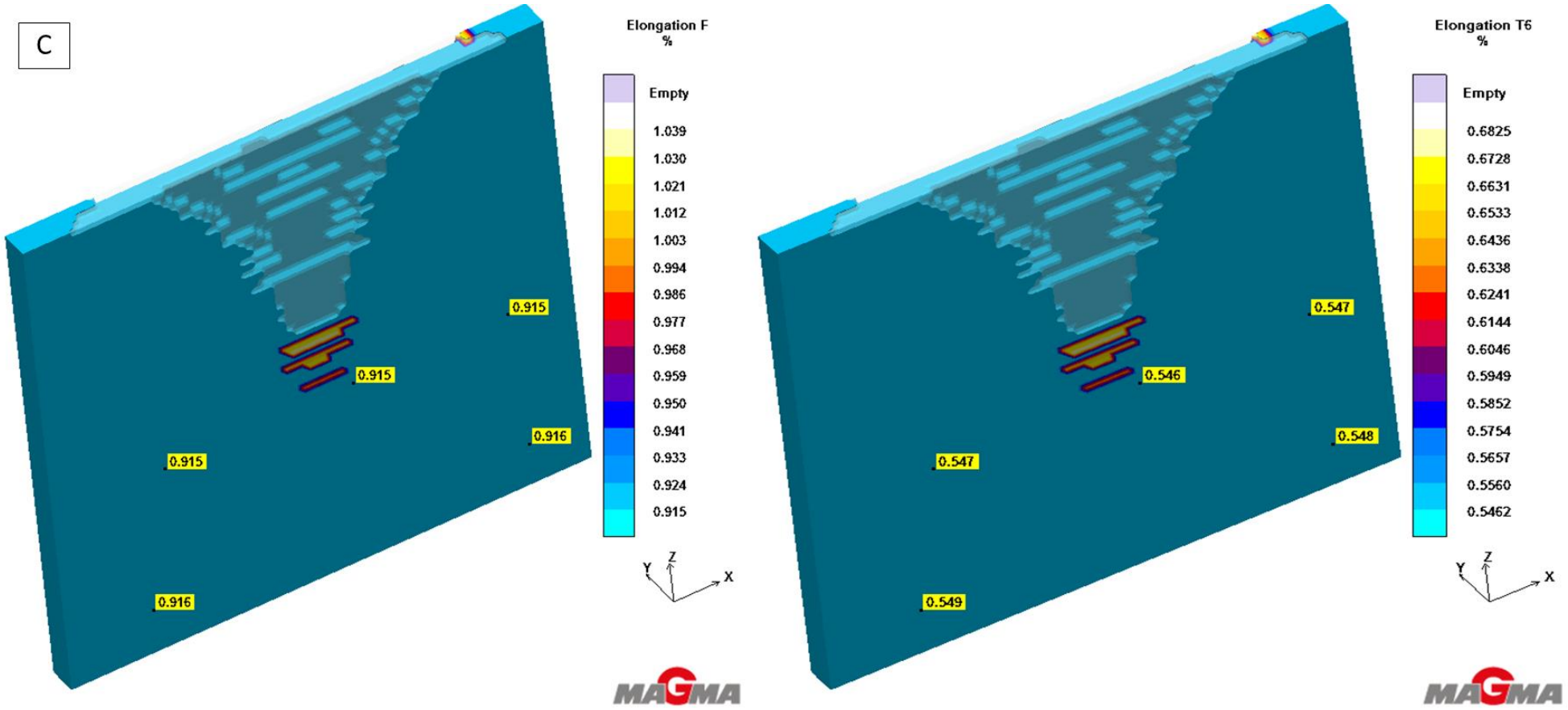

Figure 4.18: Elongation of the As-cast (F) and T6 heat treated castings for section thickness 15mm

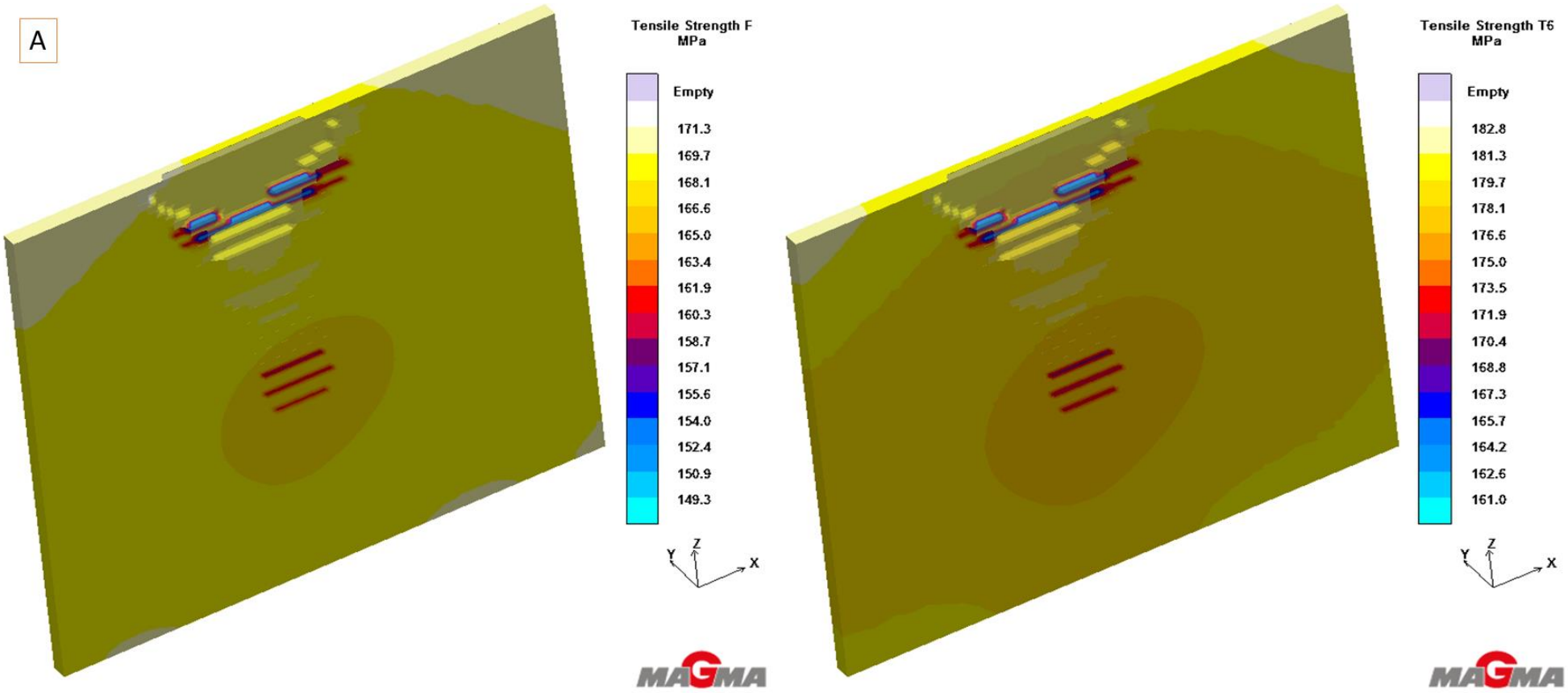

Figure 4.19: Tensile Strength of the As-cast (F) and T6 heat treated casting for section thickness 10mm

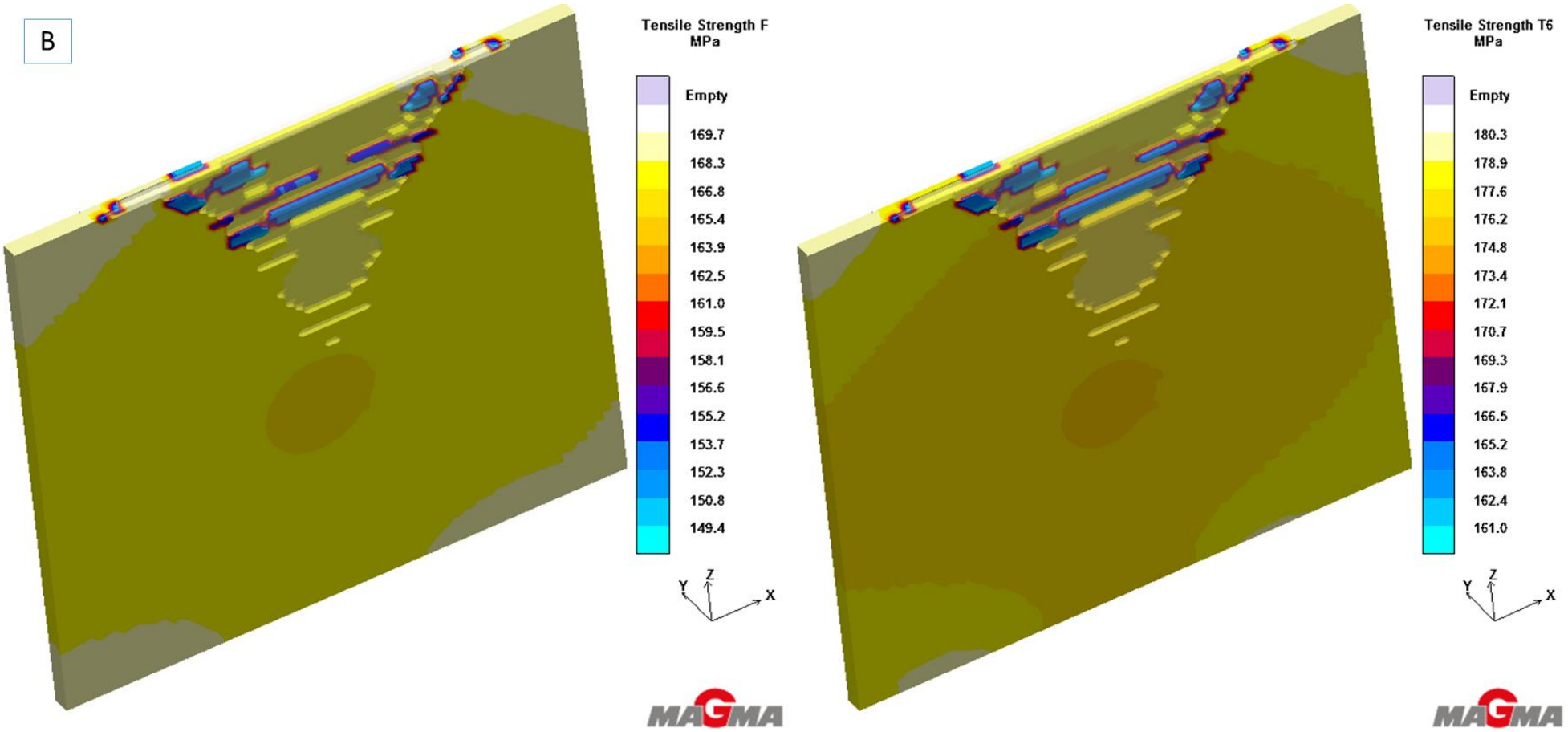

Figure 4.20: Tensile Strength of the As-cast (F) and T6 heat treated casting for section thickness 12.5mm

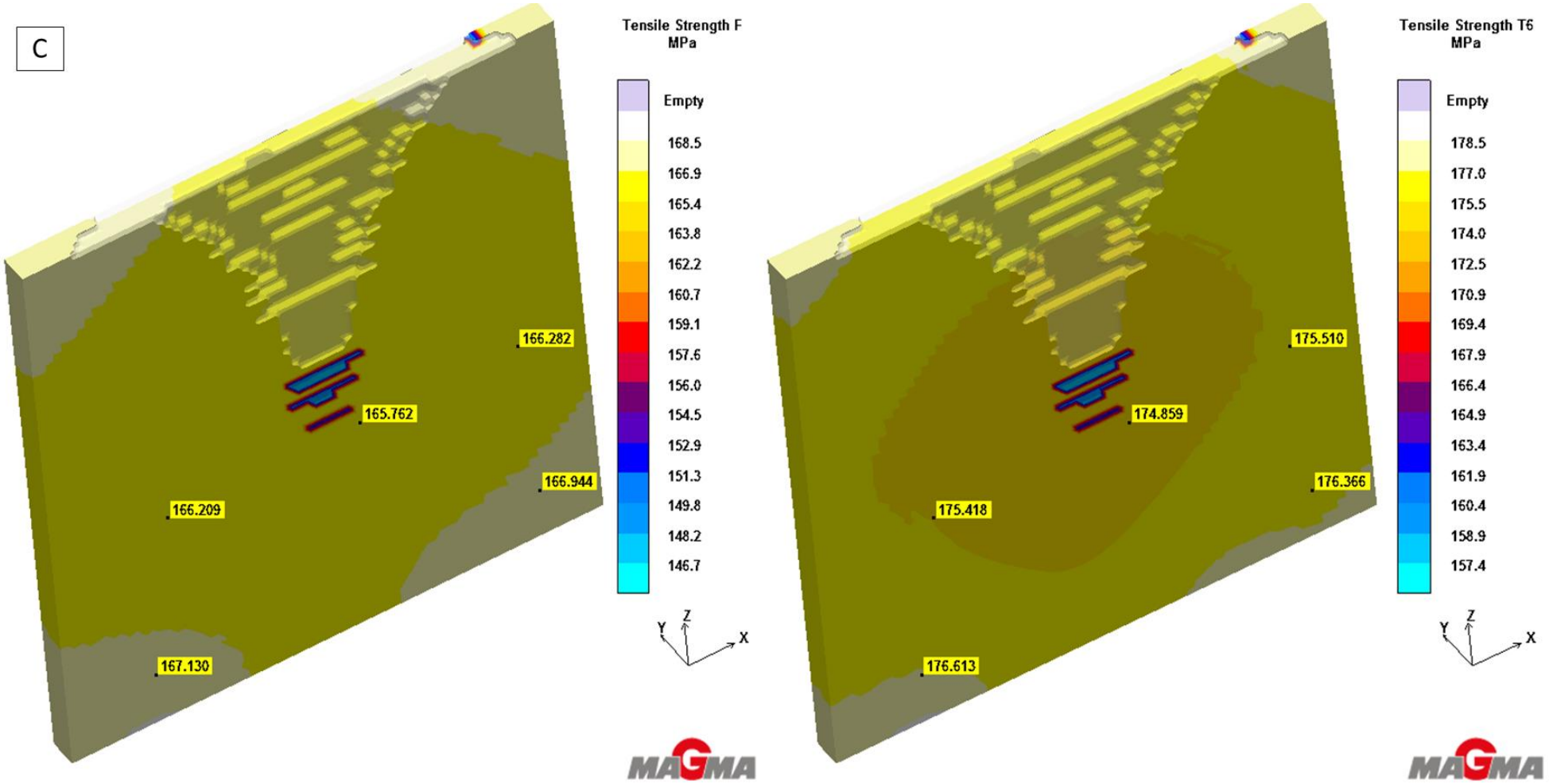

Figure 4.21: Tensile Strength of the As-cast (F) and T6 heat treated casting for section thickness 15mm

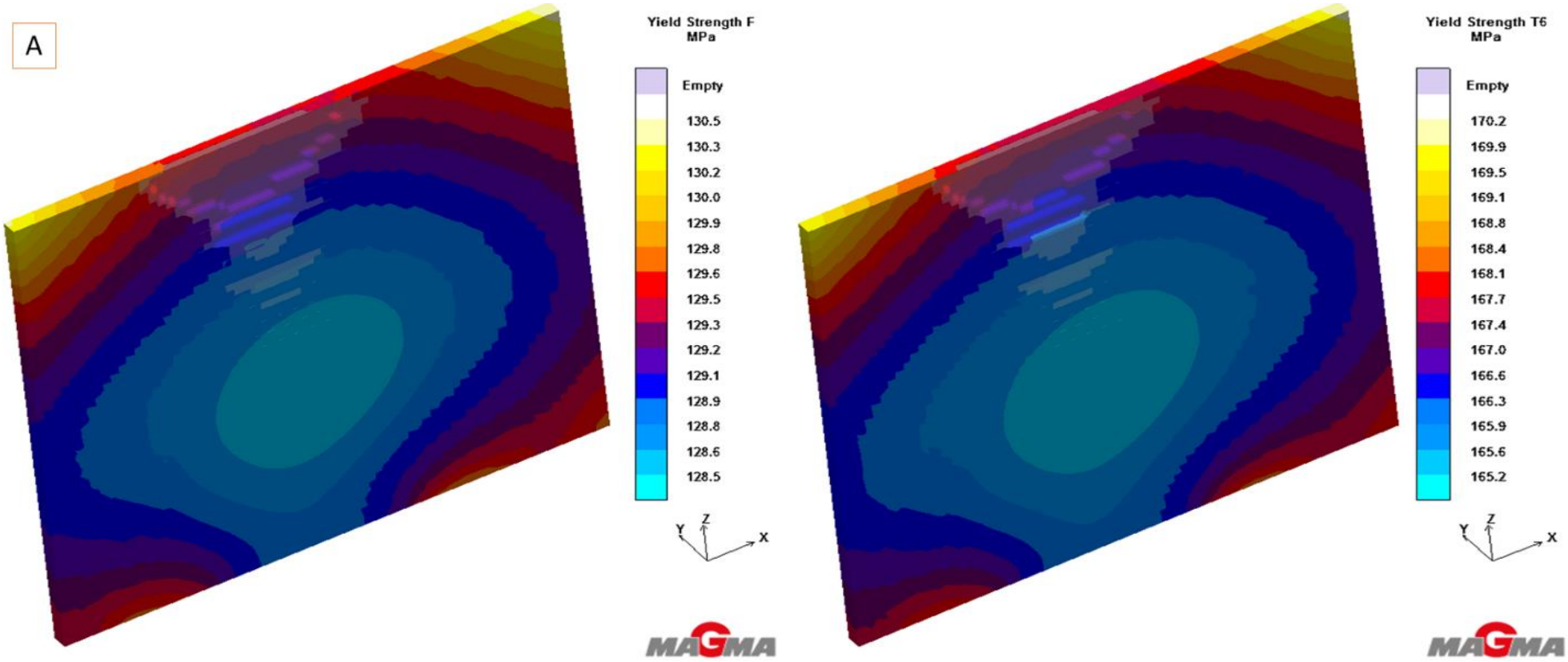

Figure 4.22: Yield Strength of the As-cast (F) and T6 heat treated casting for section thickness 10mm

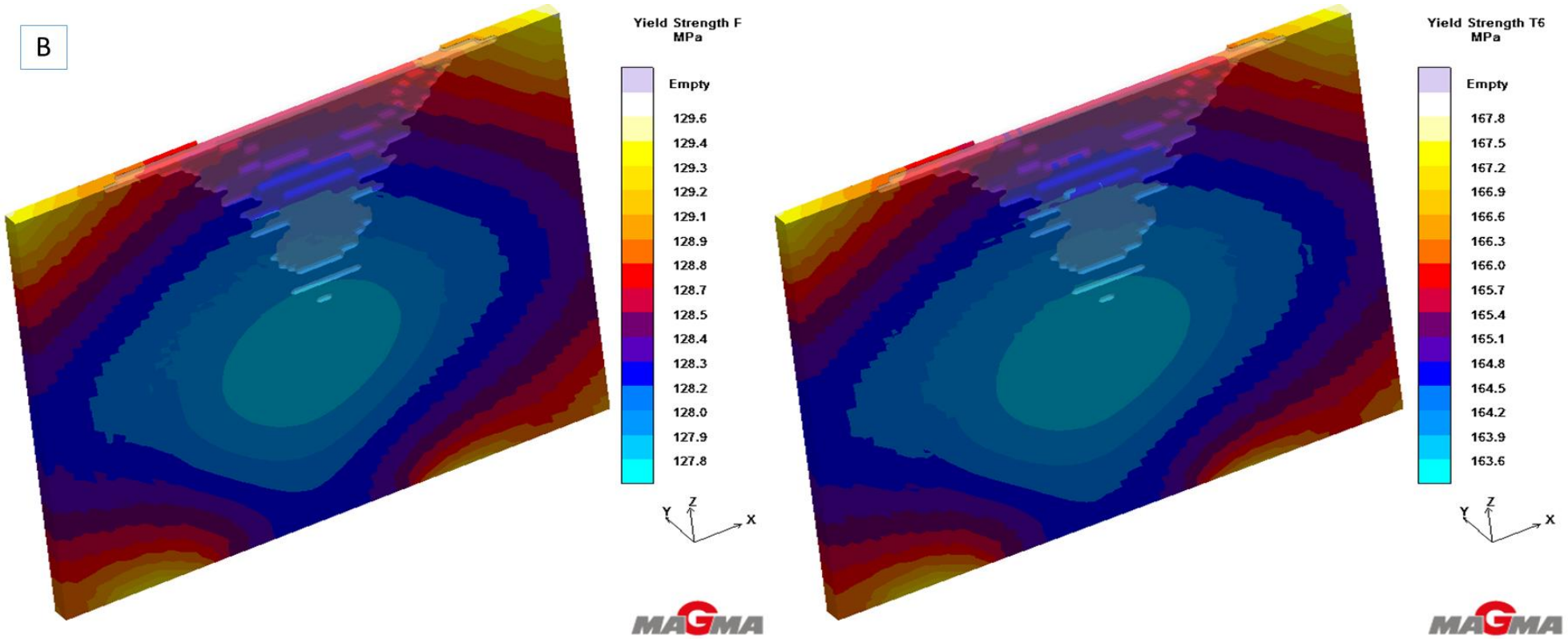

Figure 4.23: Yield Strength of the As-cast (F) and T6 heat treated casting for section thickness 12.5mm

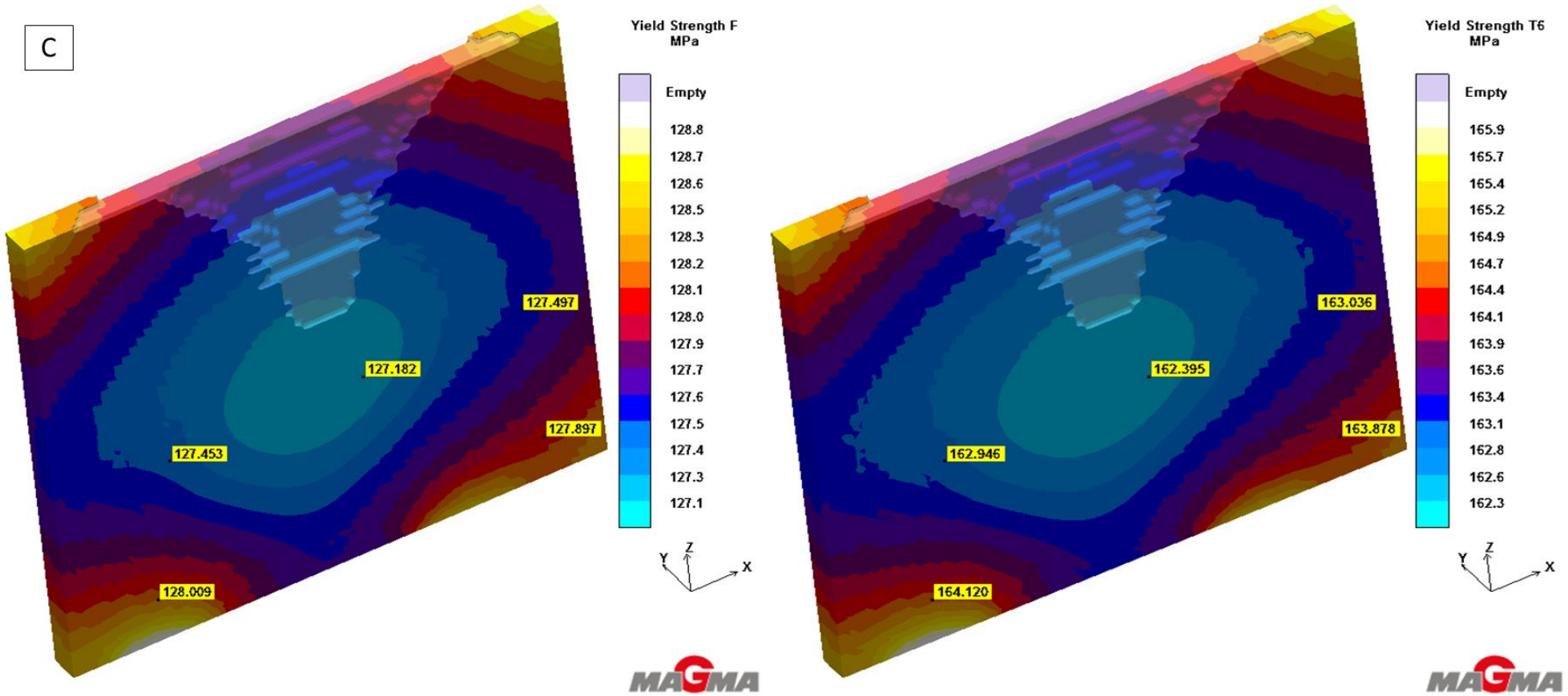

Figure 4.24: Yield Strength of the As-cast (F) and T6 heat treated casting for section thickness 15mm

4.2. Experimental Results

Porosity was very severe in the casting as can be observed on the surface of samples after final polishing (Figure 4.25). During the casting of the samples, it can be observed from the cooling curves (Figures 4.26 - 4.28), that the time required for cooling is longer as the section thickness increases. This definitely has an effect on the microstructure and porosity, as previously indicated. It was observed that the faster cooling rate 10mm casting had less porosity than the other castings with slower cooling.

Other important temperature values obtained from the first derivative of the cooling curve were the following (as numbered on the graphs, (Figures 4.26 - 4.28) :

1. Nucleation of Al dendrite networks at about 598°C
2. Nucleation of Al-Si eutectic at about 553°C
3. Nucleation of Cu-rich phases at about 496°C

It should be noted, that after a meticulous study of the temperature data per casting, it was found that the temperature in the centre of the mould ranged between 650-710°C during pouring. This temperature increased with section size, as it is obvious that more molten metal will be around the thermocouple. With the exception of the first 10mm casting, all other castings showed extreme porosity. The highest temperature registered for this first casting was about 606°C, which leads to the conclusion that for sections thicker than 10mm, the pouring temperature needs to be low enough to allow for a faster cooling in order to reduce the porosity.

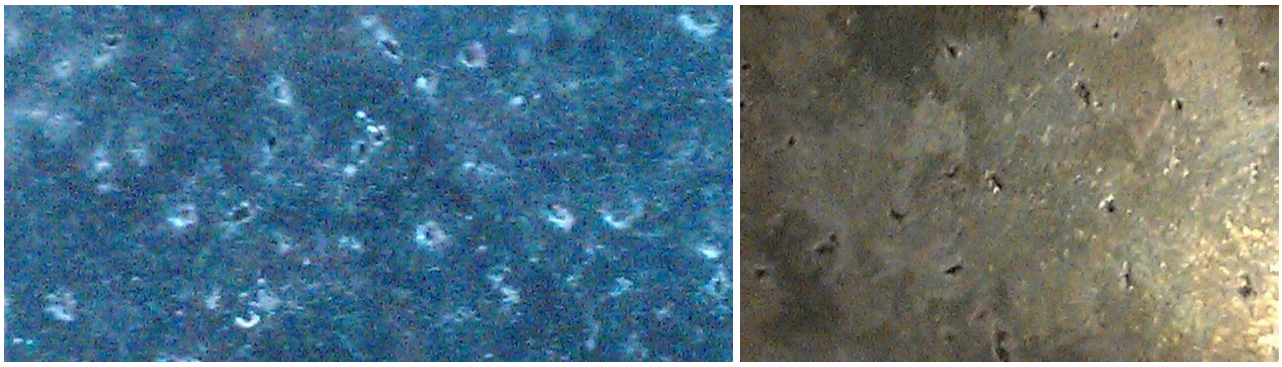

Figure 4.25: Visible porosity cavities on surfaces of samples from the 13mm (right) and 15mm casting (left), and from the samples 1 and 4, respectively, as indicated in figure 3.6.

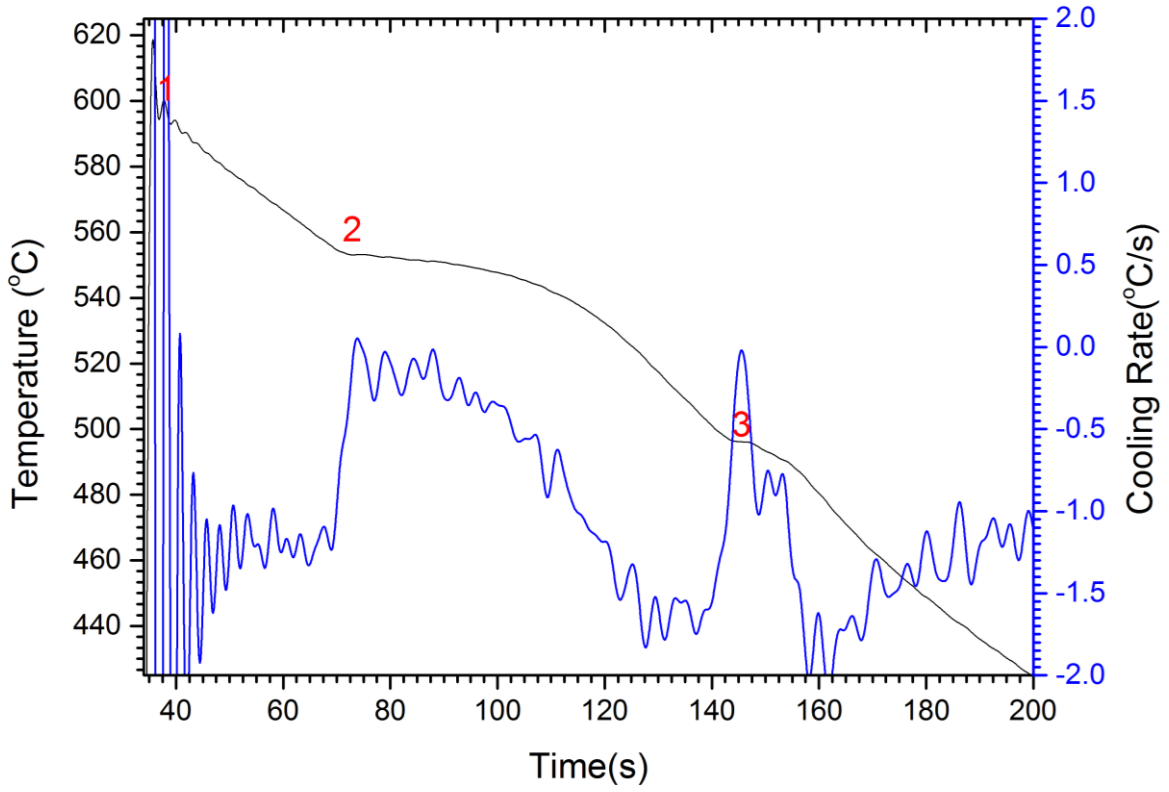

Figure 4.26: Cooling curve (black line) and cooling rate curve (blue line) registered at the centre of 10mm casting; points 1, 2 and 3 indicate nucleation of Al dendrite network, Al-Si eutectic and Cu-rich phases, respectively

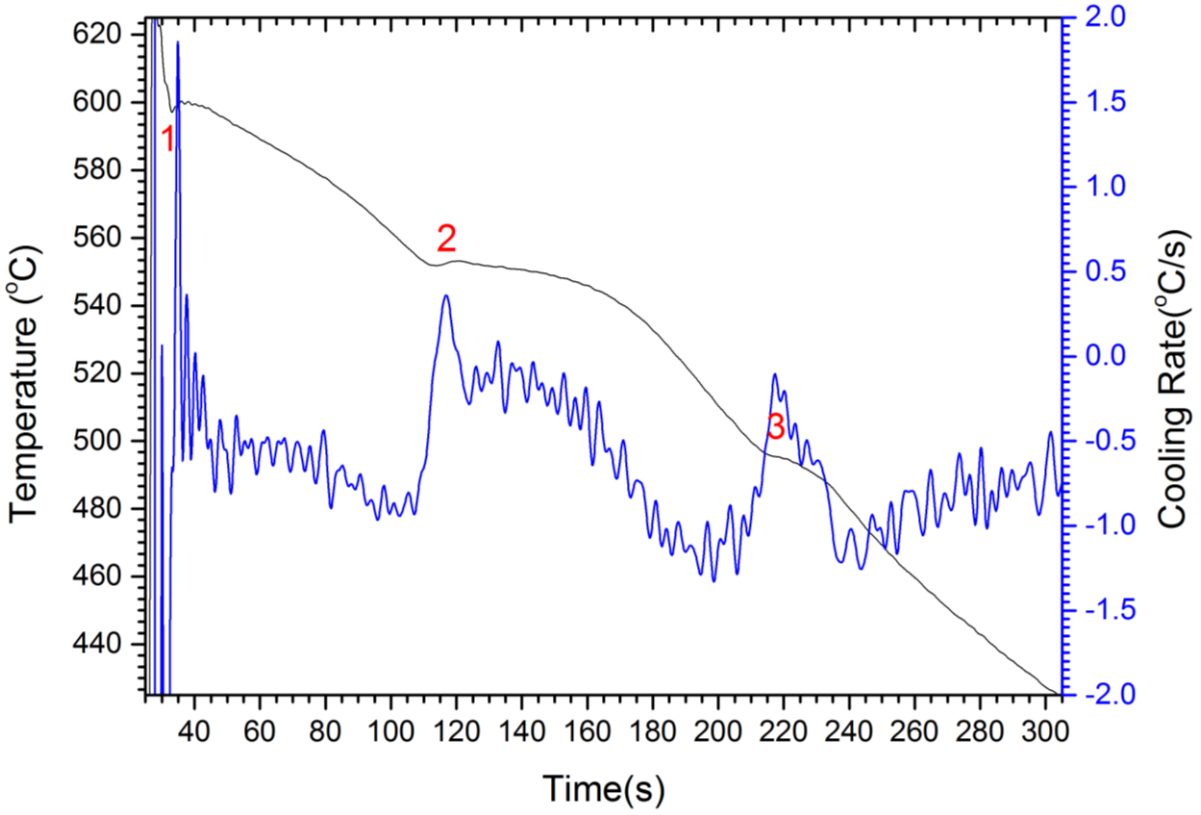

Figure 4.27: Cooling curve (black line) and cooling rate curve (blue line) registered at the centre of 12.5mm casting; points 1, 2 and 3 indicate nucleation of Al dendrite network, Al-Si eutectic and Cu-rich phases, respectively

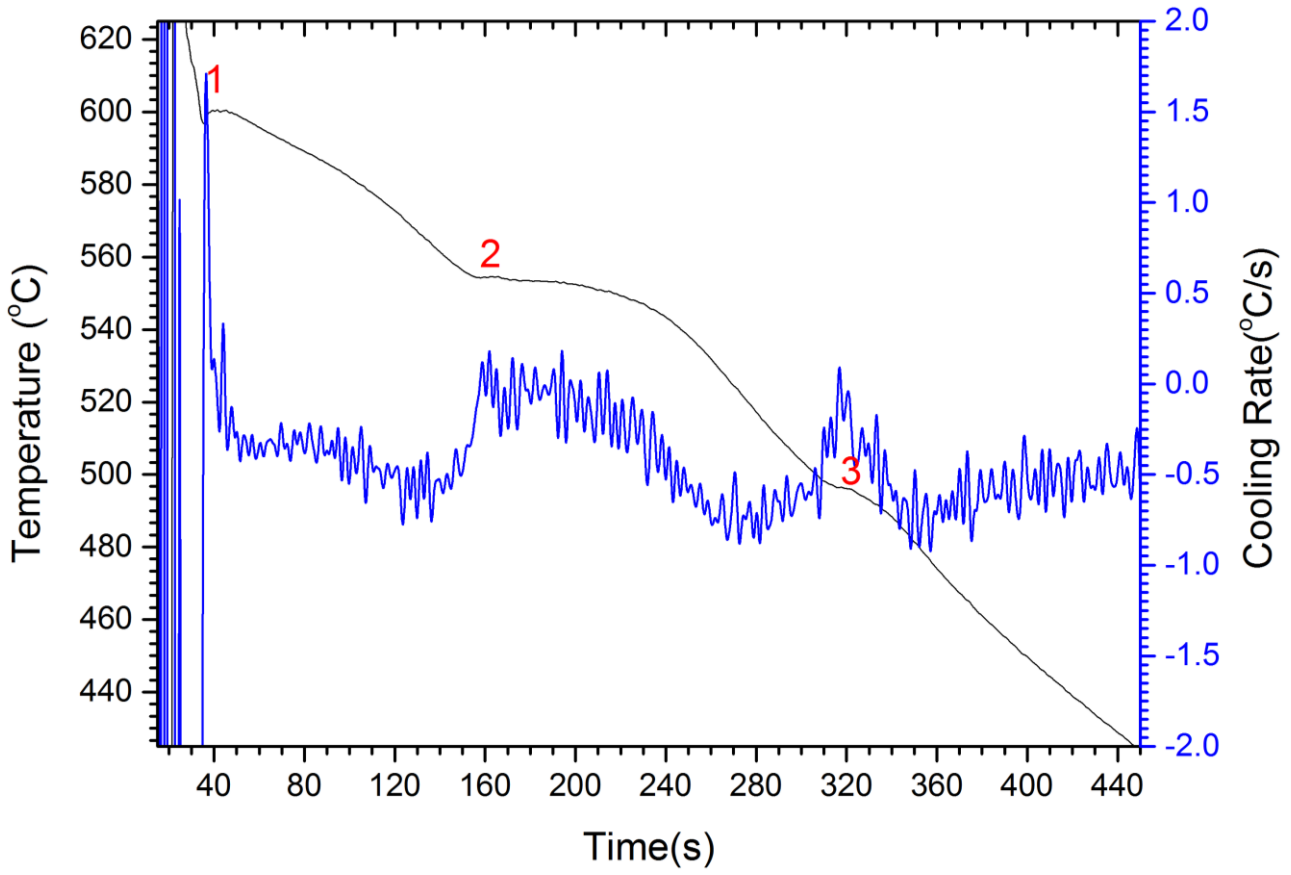

Figure 4.28: Cooling curve (black line) and cooling rate curve (blue line) registered at the centre of 15mm casting; points 1, 2 and 3 indicate nucleation of Al dendrite network, Al-Si eutectic and Cu-rich phases, respectively

4.3. Microstructural Analysis

Six samples of each of the section sizes, including the heat treated specimens, were sent for X-ray diffraction for the identification of phases (Figure 4.29). From the analysis, the solid solution α-Aluminium matrix, the eutectic Silicon, the intermetallic Al_2Cu and FeSi phases were identified from the XRAYAN software's database. It should be noted that the FeSi phase was observed very close to some high Al peak. It can be assumed that this is the AlFeSi phase that is mentioned in literature. The intensity of the phases can be attributed to the low element composition and length of the XRD test.

Further analysis was done under an optical microscope, after samples had been etched in a Keller etchant. Observational comparisons were made with literature, for the identification of phases. The as-cast microstructure (Figure 4.30), clearly shows the detrimental needle-like Si phase, as well as the Al_2Cu phase, but the AlFeSi phase was difficult to identify, due to the lack of literature. The "Chinese-script" Fe-rich phases were identified, although with some ambiguity (Figure 4.31).

The heat treated samples (Figure 4.32) had the textbook spheroidise Si present. The Al_2Cu phase was not observed at all, and it can only be assumed that it had dissolved into the matrix. The difficulty to dissolved possible Fe-rich phases was identified. This was observed by Tillova et al. [74], and showed the fragmentation of this phase, which can be due to the higher solution heat treatment temperature. In Figure 4.33, another possible phase Al-Al_2Cu-Si was noticed, which had also been described and depicted by Tillová et al [74]. This phase was described in literature as to nucleate on small eutectic Si-particles. This can be identified as the Oswald ripening phenomena.

Other phases, such as Mg_2Si, the insoluble $FeAl_3$ or $FeMnAl_6$, were not observed in the as-cast or the heat treated micrographs or by XRD analysis.

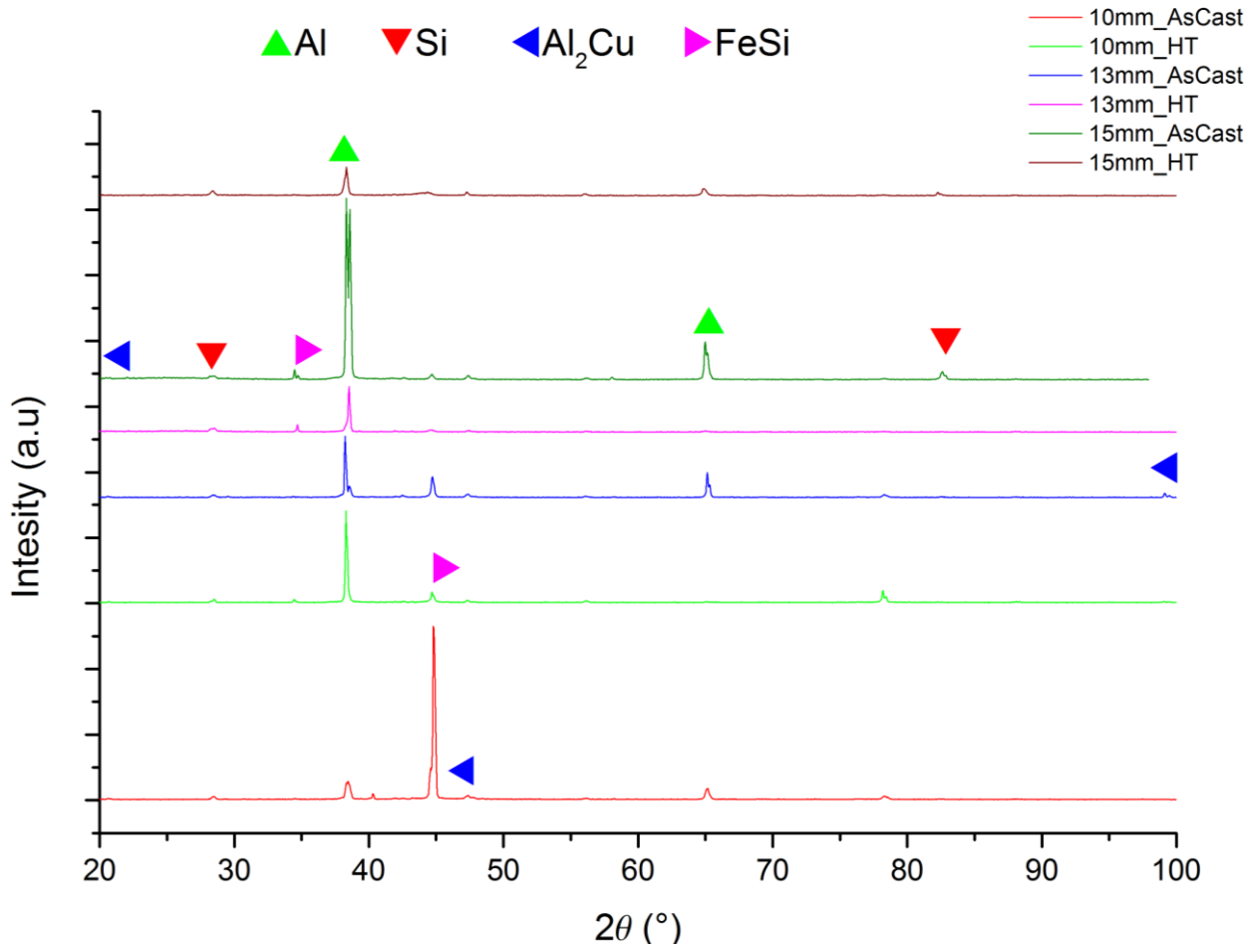

Figure 4.29: X-ray Diffraction analysis of specimens

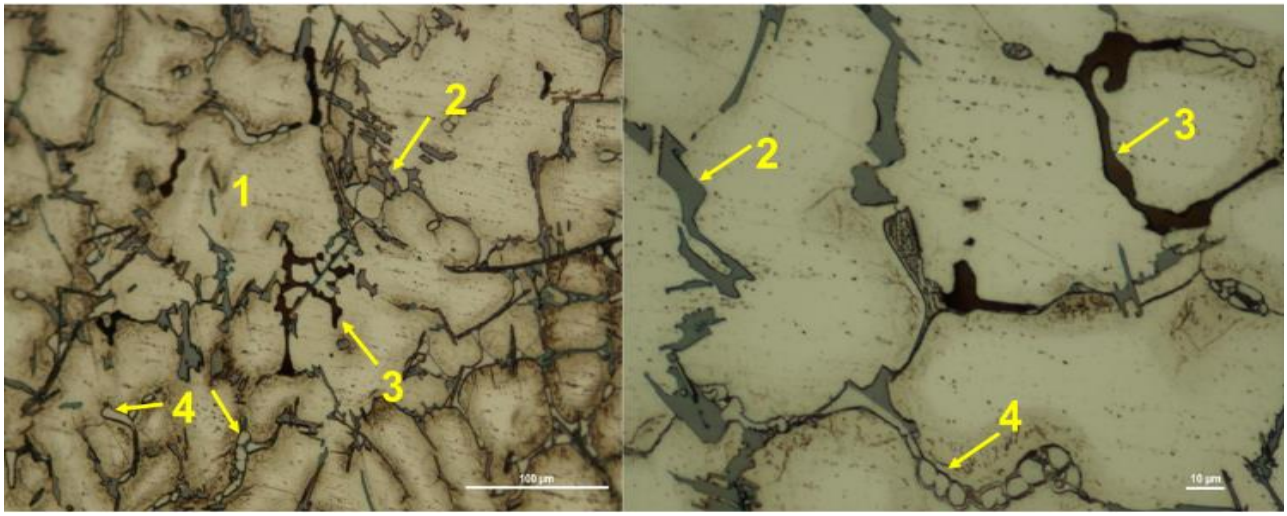

Figure 4.30: As-cast microstructure showing 1) α-Al; 2) Needle-like Silicon; 3) Al_2Cu phase; 4) AlFeSi phase. (Sample etched for 90seconds; right micrograph: x20 magnification; left micrograph: x50 magnification).

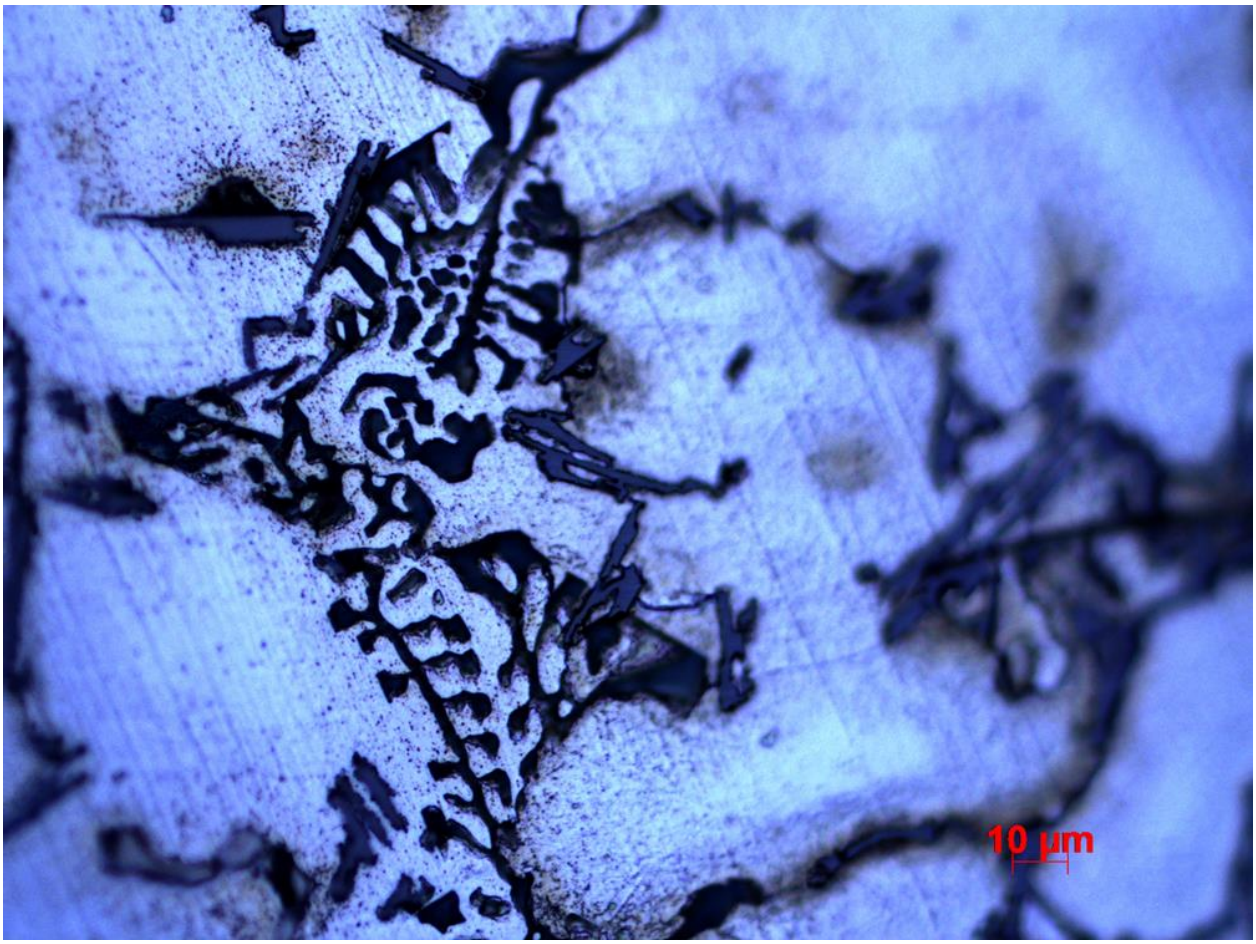

Figure 4.31: As-cast microstructure showing "Chinese-script" Fe-rich phase (x50 magnification.)

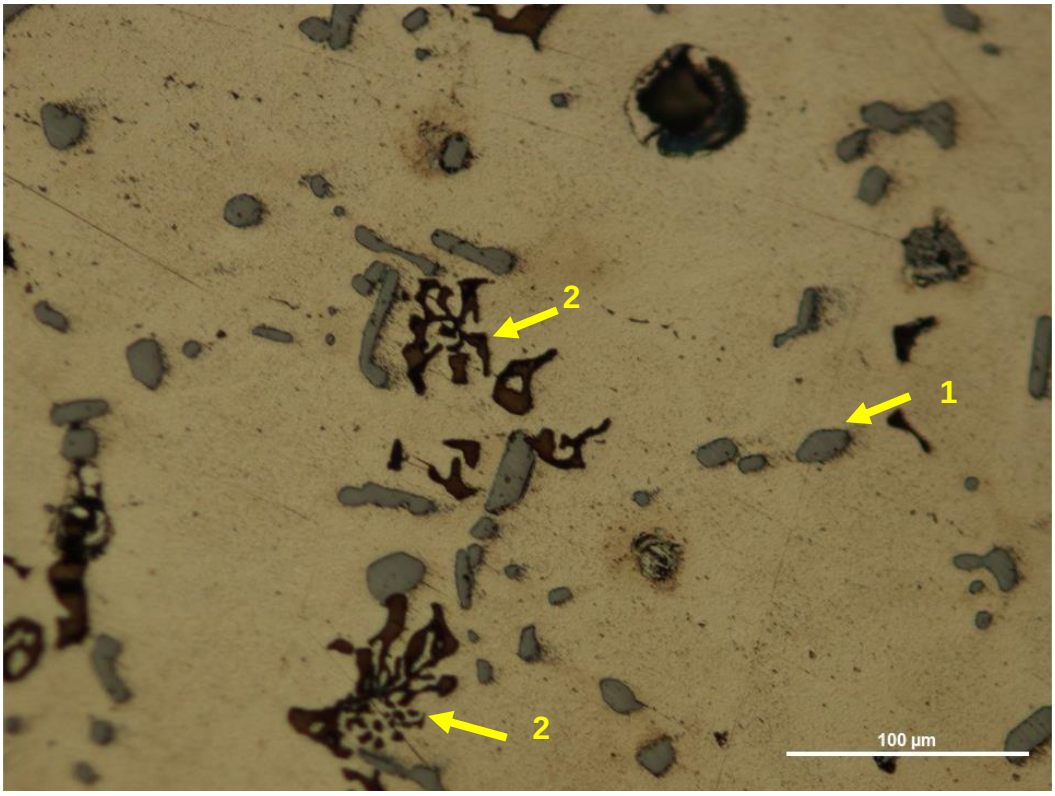

Figure 4.32: Microstructure of heat treated sample showing 1) Spheroidise Silicon; 2) Fragmentation, segmentation and dissolution of Fe-rich phases. (Sample etched for 60seconds; x20 magnification).

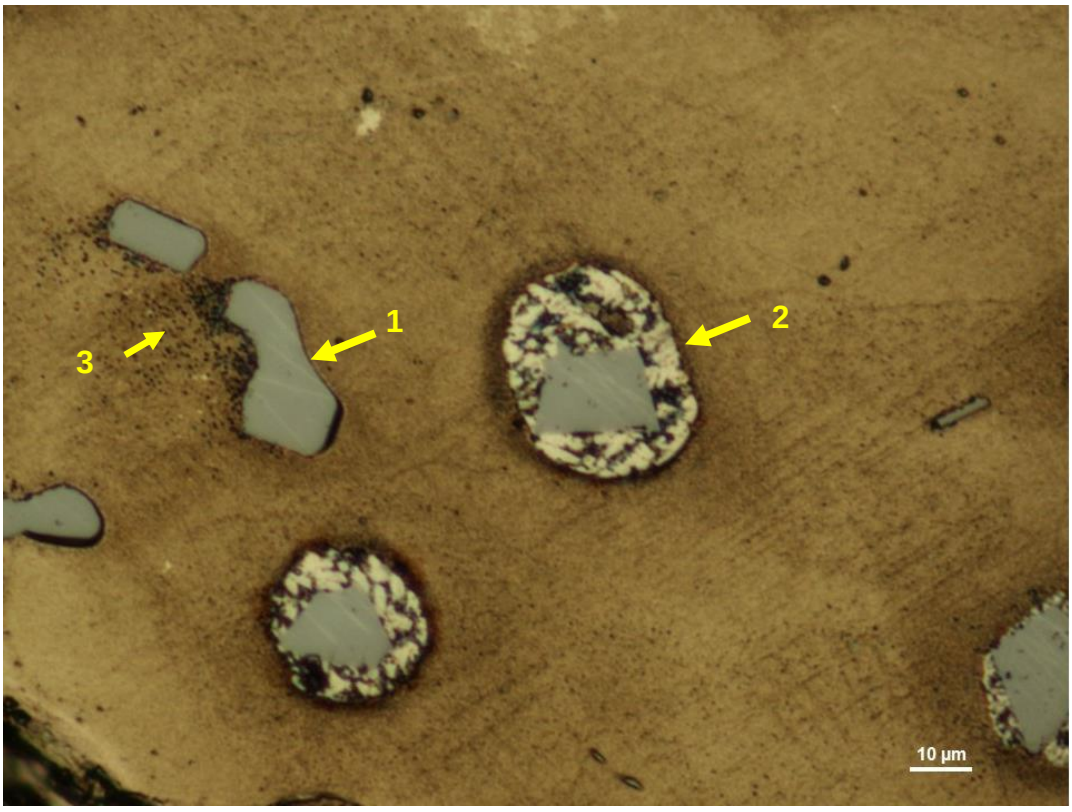

Figure 4.33: Microstructure of heat treated sample showing 1) Spheroidise Silicon; 2) Possible Al-Al_2Cu-Si phase with homogeneous shape; possible dissolution of Mg_2Si phase. (Sample etched for 90seconds; x50 magnification).

The SEM spot analysis (Figure 4.34 and Table 4.1), revealed the Mg-containing phases, which seems to appear near Al_2Cu particles. The analysis also indicated complex particles such as spots 2 and 4, appearing as lamellae. A line analysis (figure 4.35) showed a spike, which can be a possible Mg_2Si phase, on an Al_2Cu phase. An additional area and spot analysis on another particle (figure 4.36 and table 4.1) strengthens this assumption.

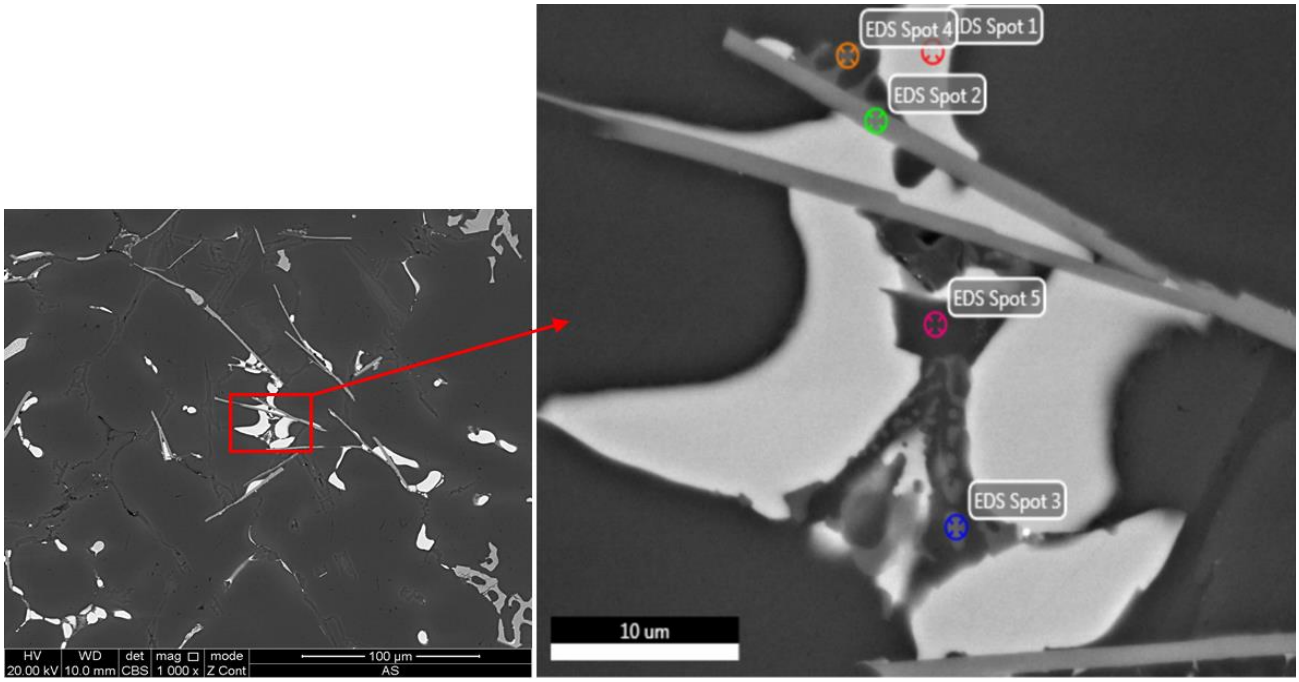

Figure 4.34: SEM micrograph of the as-cast microstructure, indicating the region (left) for spot analysis (right).

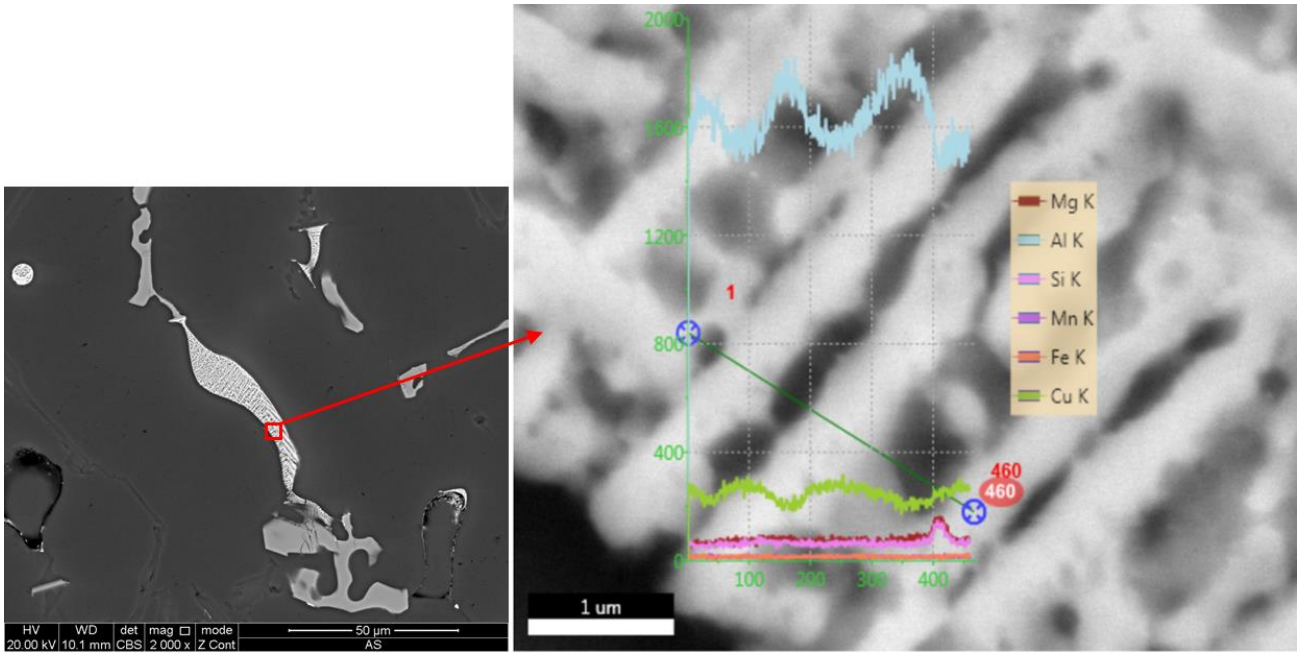

Figure 4.35: SEM micrograph of the as-cast microstructure, indicating the region (left) for line analysis (right)

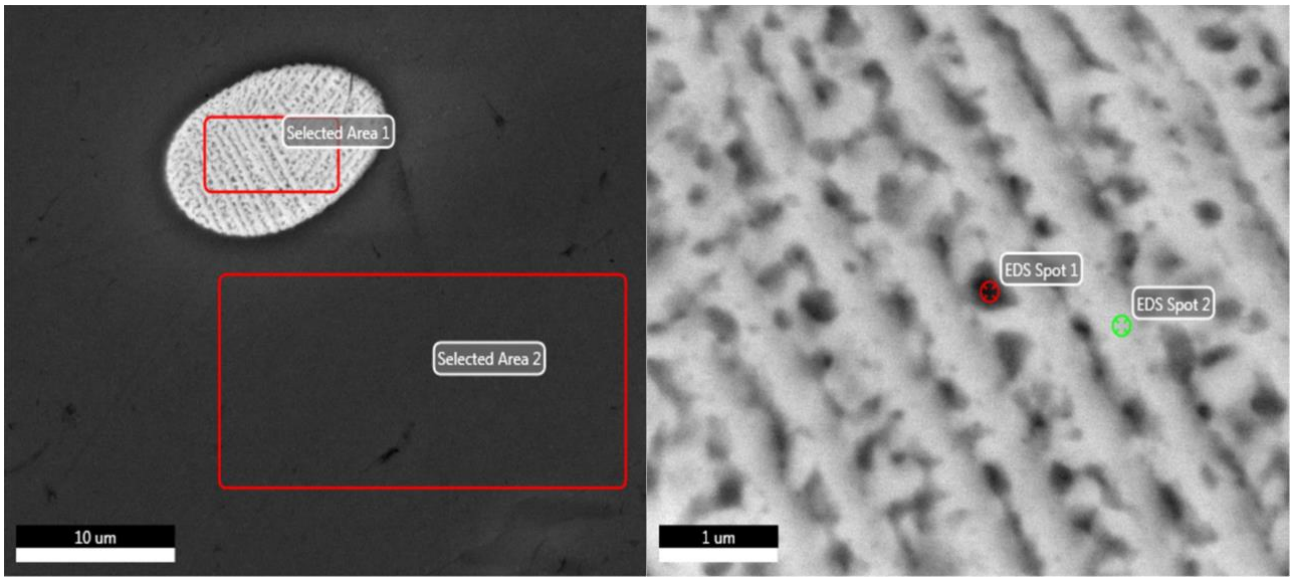

Figure 4.36: SEM micrograph of the as-cast microstructure, indicating the regions (left) for area analysis, and spot analysis (right) on the Selected Area 1 (left).

The SEM analysis on the heat treated sample (Figure 4.37), showed the presence of the strengthening Al_2Cu phase (Spot 1), the complex Fe-rich intermetallic phases (Spot 2 and 3), and the spheroidised Si (Spot 4). An area analysis (Selected Area 1) exposed the assumed Oswald ripening phenomenon, with the Mg-Si phase embedded on the Al-Cu intermetallic. A closer analysis (Figure 4.38), strengthens the notion, but is indicative of a much richer phase with Al-Cu-Si as the main elements. The above analysis is supported in Table 4.1.

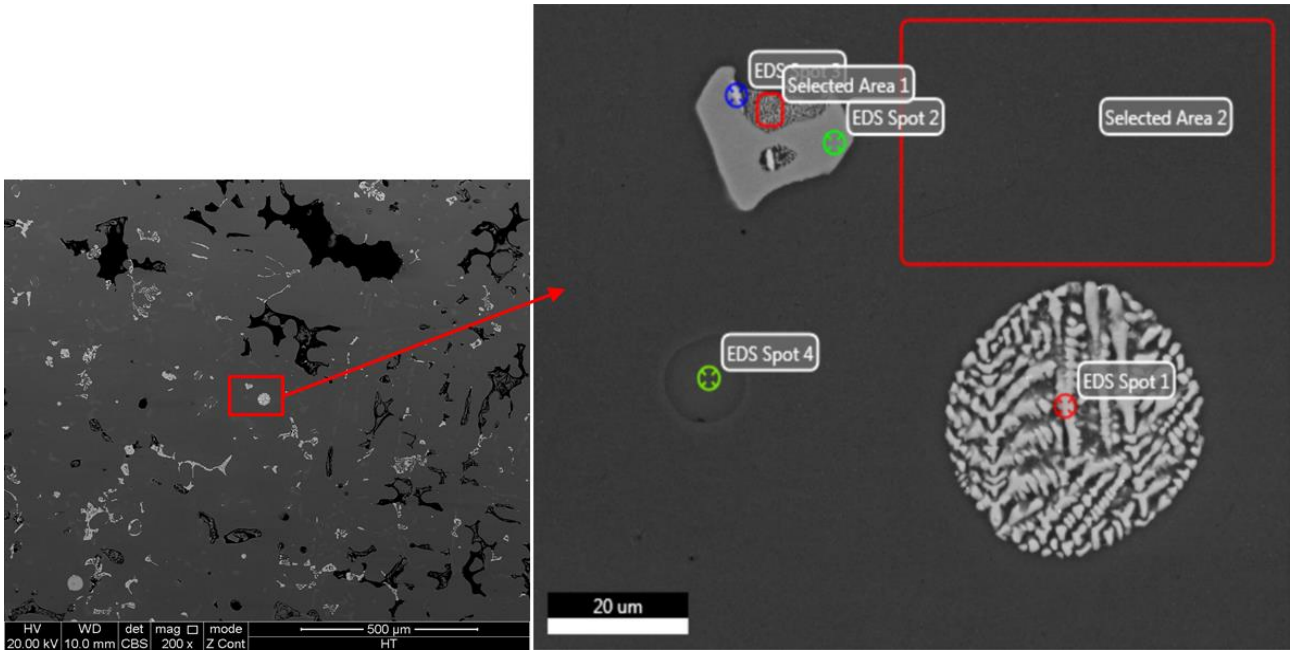

Figure 4.37: SEM micrograph of the heat treated microstructure, indicating the region (left) for spot and area analysis (right).

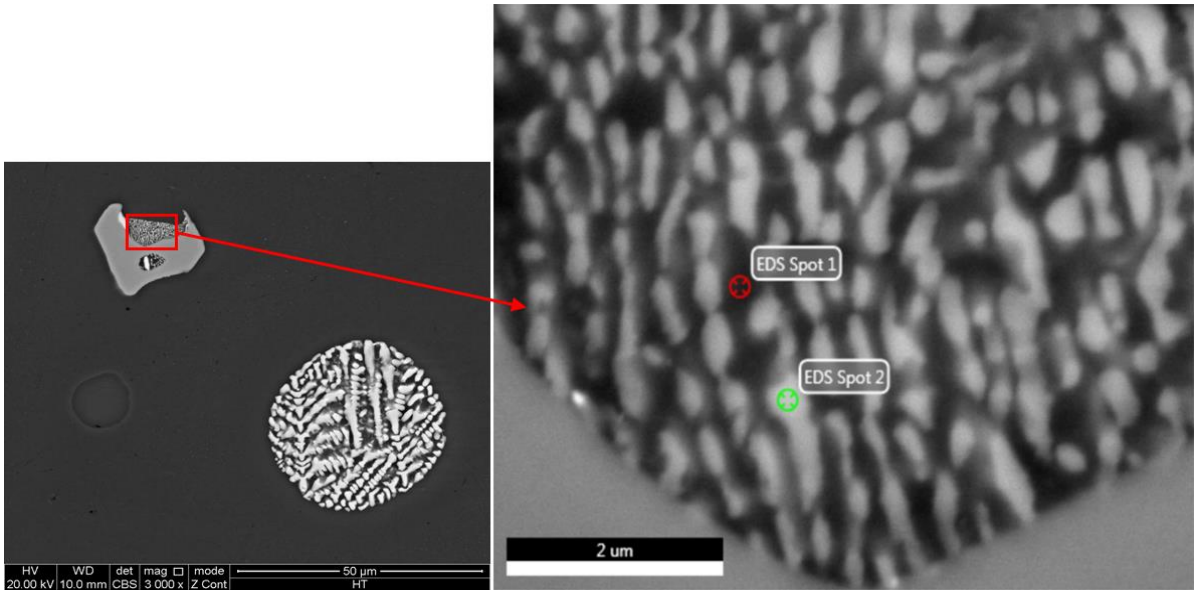

Figure 4.38: SEM micrograph of the heat treated microstructure, indicating the region (left) for spot analysis (right).

Further analysis of the heat treated microstructure also exposed the “Chinese-script” Fe rich phases, as depicted in Figure 4.39 (analysis in Table 4.1), but also rich in Mn. A lead (Pb) impurity was also detected by the analysis (Spot 2).

A line analysis (Figure 4.40) shows the close packing of elements around the Fe-particle, indicating the complexity, which leads to the difficult insolubility of these phases.

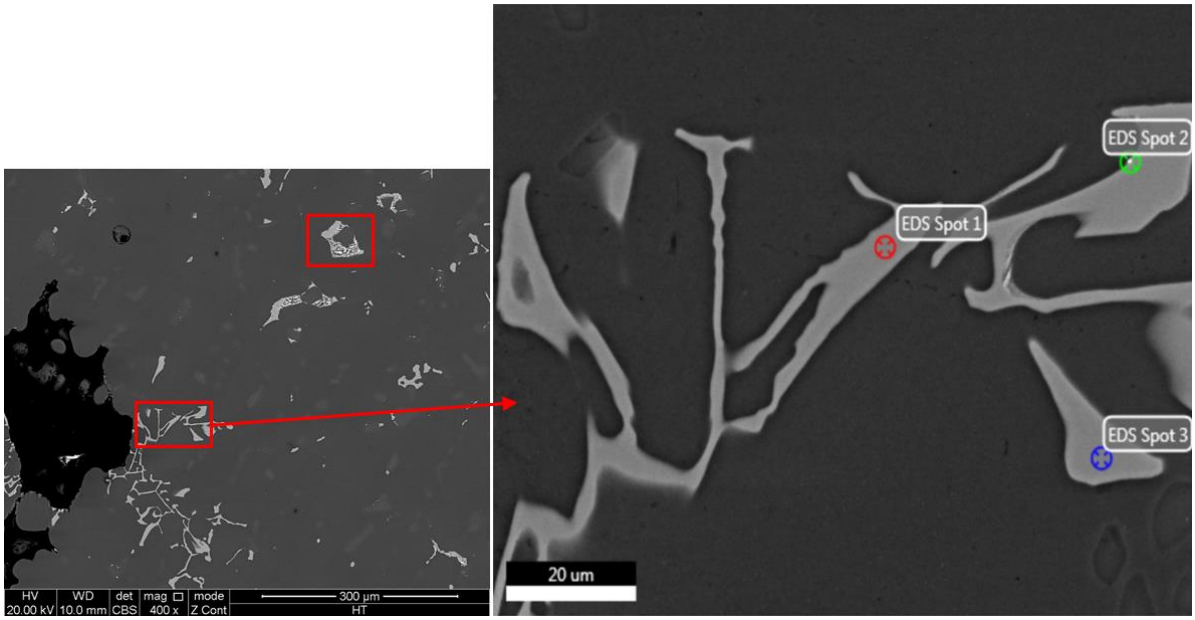

Figure 4.39: SEM micrograph of the heat treated microstructure, indicating the region (left) for spot analysis (right).

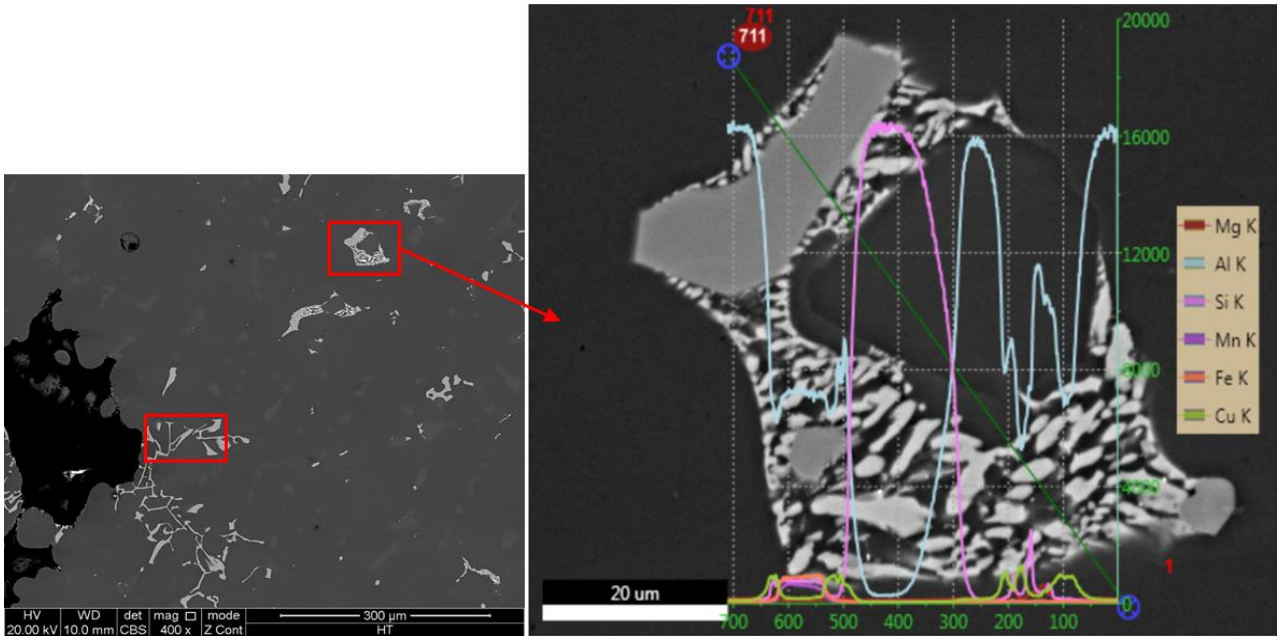

Figure 4.40: SEM micrograph of the heat treated microstructure, indicating the region (left) for line analysis (right)

The final analysis was conducted on an Al-Fe-Mn-Si-Cu phase (Figure 4.41) with an Al-Mg-Cu-Fe-Si-Mn particle on edge (Spot 1). This is an intriguing particle, as the Mg wt% is higher than the Cu, which can be described as the Al_2Cu phase.

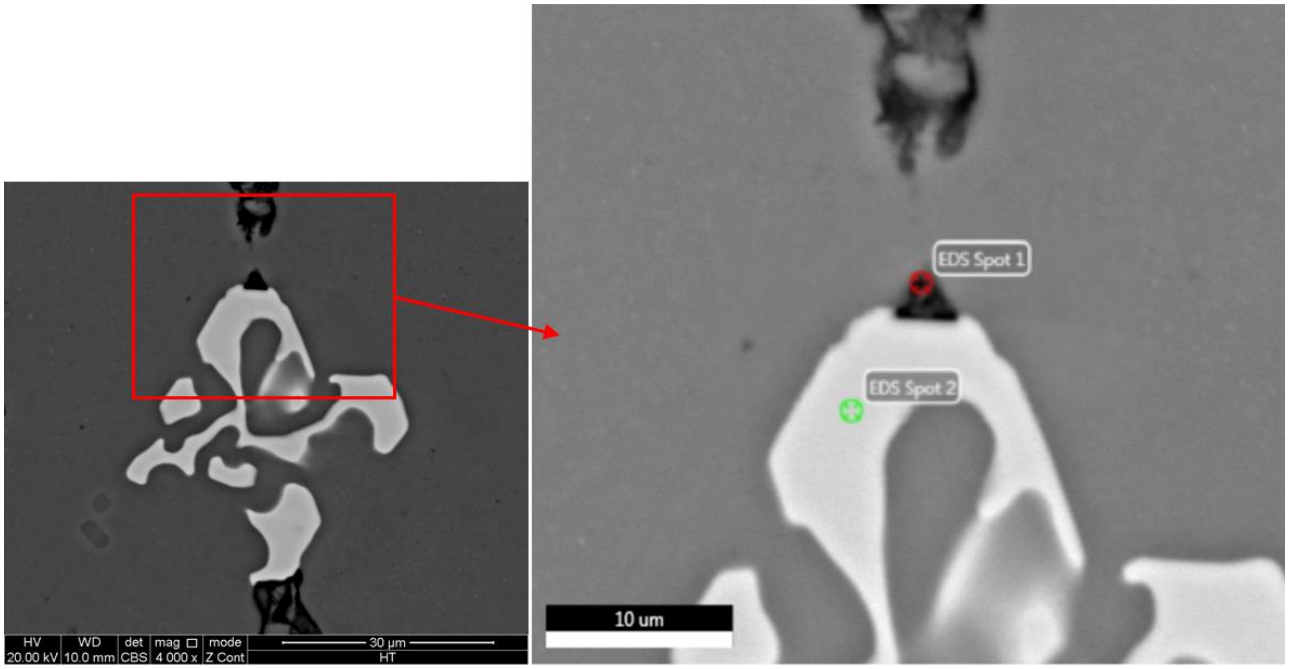

Figure 4.41: SEM micrograph of the heat treated microstructure, indicating the region (left) for spot analysis (right).

Table 4.1: Compositional analysis from SEM

	Element (wt%)		Al	Cu	Fe	Mg	Mn	O	Si
As-cast microstructure	Figure 4.34	Spot 1	53.35	45.65	-	-	-	0.15	0.85
		Spot 2	54.16	11.13	13.35	1.18	5.01	-	15.16
		Spot 3	52.63	14.5	-	15.62	-	-	17.25
		Spot 4	60.97	10.89	1.02	11.7	-	-	15.42
		Spot 5	29.5	3.7	-	0.78	-	-	66.05
	Figure 4.36	Area 1	53.42	40.65	0.63	2.7	-	-	2.61
		Area 2	96.21	1.1	-	0.77	-	-	1.92
		Spot 1	55.54	39.44	0.57	2.24	-	-	2.22
		Spot 2	52.24	41.2	0.54	3.26	-	-	2.76
Heat Treated microstructure	Figure 4.37	Area 1	68.22	21.88	-	1.55	-	-	8.34
		Area 2	95.15	2.86	-	0.77	-	-	1.22
		Spot 1	53.2	41.1	0.68	-	-	-	4.3
		Spot 2	56.62	4.98	17.43	-	11.75	-	9.22
		Spot 3	57.9	35.72	1.5	0.39	0.89	0.1	3.51
		Spot 4	2.17	0.52	-	-	-	-	97.3
	Figure 4.38	Spot 1	61.14	21.3	0.56	1.11	0.28	-	15.61
		Spot 2	60.76	29.92	0.8	1.98	0.42	-	6.12
	Figure 4.39	Spot 1	56.38	4.65	16.54	-	13	-	9.43
		Spot 2	60.1	7.63	6.85	0.84	5.01	-	7.69
		Spot 3	56.74	4.4	17.52	-	12.06	-	9.28
	Figure 4.41	Spot 1	88.16	3.09	1.94	4.31	1.2	-	1.3
		Spot 2	56.51	4.75	17.16	-	12.3	-	9.27

Chapter 5. Conclusion and Future Work

Computer simulation software is a very powerful tool for the foundry industry, in that it allows for educated decisions to be made, for example in terms of improving the gating system of a casting to reduce porosity, which in turn improves the material properties.

The simulated results from MAGAMSOFT® predicted porosity to be in the area where specimens were taken from, and after polishing, the large open cavities were clearly visible to the naked eye. This can be attributed to the lack of a proper feeding system, which adversely causes shrinkage and macrosegregation. The cooling of the first casting is significantly faster than the others, which greatly affected the microstructure, as no visible porosity could be seen with the naked eye. Thus, it can be concluded that section size is proportional to porosity.

The metallographic study produced interesting results, both before and after heat treatment. The needle-like silicon phases were clearly visible, and after heat treatment the transformation to a spheroidal shape was observed. The higher solution heat treatment temperature of 525°C, as opposed to 520°C as recommended by literature, showed that Cu containing phases did dissolve. It was also observed that the Fe-rich phases were in the process of fragmenting and dissolving, from which can be determined that this higher temperature was beneficial, and that an extended period would have dissolved it completely.

The SEM analysis produced and revealed interesting results. More complex intermetallic phases were observed, which are rich in Fe and Mn. Also, it was found that Mg-containing phases manifest upon or near to Cu-rich or Fe-rich phases. Area analysis of the selected areas in Figures 4.36 and 4.37 (Table 4.1, area 2) indicated that dissolution of Cu occurred after heat treatment, as the Al-matrix contained an increased wt% of the element, while Mg remained constant.

The simulated material properties produced by MAGMASOFT®, could not be verified, as no mechanical testing was done. This can be a future study, as it would complete the cycle in understanding the effects of this applied heat treatment schedule on the material properties. The microstructural analysis through SEM can then possibly reveal the Friedel effect and/or Orowan mechanisms.

It can be finally concluded that to improve the microstructure, and to reduce defects, a better gating and feeding system needs to be designed. Also, great care should be taken in controlling the cooling rate, and therefore the external environment requires monitoring.

List of Figures

List of Tables

References

[1] Miller, W.S., Zhuang, L., Bottema, J., Wittebrood, A.J., De Smet, P., Haszler, A., Vieregge, A., "Recent development in aluminium alloys for the automotive industry," *Materials Science and Engineering A,* vol. 280, no. 1, pp. 37-49, 2000.

[2] Kaufman, J.G., Rooy, E.L., Aluminum Alloy Castings Properties, Processes, and Applications, 1st ed., A. International, Ed., Ohio, USA: ASM International, 2004.

[3] Gopikrishna, S., Binu, C.Y., "Study on effects of T6 heat treatment on grain refined A319 alloy with Magnesium and Strontium addition," *International Journal on Theoretical and Applied Research in Mechanical Engineering,* vol. 2, no. 3, pp. 59-62, 2013.

[4] Kearney, A.L., "Properties of Cast Aluminum Alloys," in *ASM Handbook Volume 2 Properties and Selection: Nonferrous Alloys and Special-Purpose Materials*, 10th ed., vol. 2, ASM International, 1992, pp. 569-666.

[5] Heusler, L.,Feikus, F.J., Otte, M.O., "Alloy and Casting Process Optimization for Engine Block Application," *AFS Transaction,* vol. 1, no. 50, pp. 1-9, 2001.

[6] Hirsch, J., "Automotive Trends in Aluminium - The European Perspective," *MATERIALS FORUM,* vol. 28, pp. 15-23, 2004.

[7] Mohamed, A.M.A., Samuel, F.H, "A Review on the Heat Treatment of Al-Si-Cu/Mg casting alloys," in *Heat Treatment*, Rijeka, Croatia, InTech Science, 2012, pp. 229-246.

[8] Sjölander, E., Seifeddine, S. , "Optimisation of solution treatment of cast Al–Si–Cu alloys," *Materials and Design,* vol. 31, no. SUPPL. 1, pp. S44-S49, 2010.

[9] Rooy, E.L., "Aluminum and Aluminum Alloys: Chemical Compositions," in *ASM Handbook Volume 15: Castings*, ASM International, 1992, pp. 1622-1631.

[10] Rooy,E.L., "Aluminum and Aluminum Alloys: Effects of Alloying Elements," in *ASM Handbook Volume 15: Castings*, ASM International, 1992, pp. 1631-1634.

[11] Polmear, I.J., Light Alloys: From Traditional Alloys to Nanocrystals, 4th ed., Oxford: Butterworth-Heinemann, 2006.

[12] Brown, J.R., Foseco Non-Ferrous Foundryman's Handbook, 11th ed., Oxford: Butterworth-Heinemann, 1994.

[13] Samuel, F.H.,Samuel,A.M. ,Doty, H.W. , "Factors Controlling the Type and Morphology of Cu-Containing Phases in 319 Al Alloy," *AFS Transactions,* vol. 30, p. 893–901, 1996.

[14] Djurdjevic, M., Stockwell, T., Sokolowski, J., "The effect of strontium on the microstructure of the aluminium-silicon and aluminium-copper eutectics in the 319 aluminium alloy," *International Journal of Cast Metals Research,* vol. 12, no. 2, pp. 67-73, 1999.

[15] Mondolfo,L.F., Aluminum Alloys: Structure and Properties, London: Butterworth, 1976.

[16] Li, Z., Samuel, A.M., Samuel, F.H., Ravindran, C., Valtierra, S., "Effect of alloying elements on the segregation and dissolution of CuAl2 phase in Al-Si-Cu 319 alloys," *Journal of Materials Science,* vol. 38, no. 6, pp. 1203-1218, 2003.

[17] Samuel, A.M., Gauthier, J., Samuel, F.H., "Microstructural aspects.of the dissolution and melting of Al2Cu phase in Al-Si alloys during solution heatment," *Metallurgical and Materials Transactions A: Physical Metallurgy and Materials Science,* vol. 27, no. 7, pp. 1785-1798, 1996.

[18] Cáceres, C.H., Svensson, I.L., Taylor, J.A, "Strength-ductility behaviour of Al-Si-Cu-Mg casting alloys in T6 temper," *International Journal of Cast Metals Research,* vol. 15, no. 5, pp. 531-543, 2003.

[19] Krajewski, W.K., Greer, A.L., Zych, J., Buraś, J., "Effectiveness of Zn-Ti based refiner of Al and Zn foundry alloys," in *67th World Foundry Congress, Casting the Future, 2, pp. 894-903.*, Harrogate, United Kingdom, 2006.

[20] Krajewski, W.K., Haberl, K., "The effect of Ti on high-zinc al cast alloys structure and properties," *Acta Metallurgica Slovaca,* vol. 17, no. 2, pp. 123-128., 2011.

[21] Campbell, J., Castings, Oxford: Butterworths-Heinemann, 2003.

[22] Ghosh, A., "Segregation in cast products," *Sadhana - Academy Proceedings in Engineering Sciences,* vol. 26, no. 1-2, pp. 5-24, 2001.

[23] Beeley, P., Foundry Technology, Oxford: Butterworth-Heinemann, 2001.

[24] Voller, V.R., Beckermann, C., "A unified model of microsegregation and coarsening," *Metallurgical and Materials Transactions A: Physical Metallurgy and Materials Science,* vol. 30, no. 8, pp. 2183-2189, 1999.

[25] Askeland, D.R., Fulay, P.P, Wright, W.J., The Science and Engineering of Materials, Stamford: CL-Engineering, 2010.

[26] Won, Y.-M., Thomas, B.G., "Simple model of microsegregation during solidification of steels," *Metallurgical and Materials Transactions A: Physical Metallurgy and Materials Science,* vol. 32, no. 7, pp. 1755-1767, 2001.

[27] Yan, X., S. Chen, S., Xie,F., Chang,Y.A. , "Computational and experimental investigation of microsegregation in an Al-rich Al–Cu–Mg–Si quaternary alloy," *Acta Materialia ,* vol. 50, p. 2199–2207, 2002.

[28] Stefanescu, D.M., Science and Engineering of Casting Solidification, New York: Springer Science+Business Media, LLC, 2009.

[29] Gulliver, G.H., Metallic alloys, Griffen, 1922.

[30] Scheil, E., "Bemerkungen zur Schichtkristallbilding (Retrograde saturation curves)," *Zeitschrift für Metallkunde,* vol. 34, pp. 70-72, 1942.

[31] Dantzig, J.A., Rappaz, M., Solidification, Italy: EPFL Press, 2009.

[32] Brody, H.D., Fleming, M.C., "Solute redistribution in dendritic solidification," *Trans. Metall. Soc. AIME,* vol. 236, pp. 615-624, 1966.

[33] Clyne, T.W., Kurz, W, "Solute redistribution during solidification with rapid solid state diffusion," *Metallurgical transactions. A, Physical metallurgy and materials science,* vol. 12 A, no. 6, pp. 965-971, 1981.

[34] I. Ohnaka, "Mathematical analysis of solute redistribution during solidification with diffusion in solid phase," *Transactions of the Iron and Steel Institute of Japan,* vol. 26, no. 12, pp. 1045-1051, 1986.

[35] Sundman, B., Jansson, B., Andersson, J.-O., "The Thermo-Calc databank system," *Calphad,* vol. 9, no. 2, pp. 153-190, 1985.

[36] J. Miettinen, "Mathematical simulation of interdendritic solidification of low-Alloyed and stainless steels," *Metallurgical Transactions A,* vol. 23, no. 4, pp. 1155-1170, 1992.

[37] E. Flender, *MAGMASOFT,* Aachen: Magma Gmbh, 2000.

[38] Wołczyński, W., Effects of back-diffusion onto doublet structure formation and solute redistribution within alloys solidifying directionally, with or without convection, Krakow: Polish Academy of Sciences, Institute of Metallurgy and Materials Science, 2002.

[39] Lesoult, G., "Basic Concepts in Crystal Growth and Solidification," in *ASM Handbook: Castings Vol 15*, ASM International, 1992, pp. 231-235.

[40] Rontó, V., Roósz, A., "The effect of cooling rate and composition on the secondary dendrite arm spacing during solidification. Part I: Al-Cu-Si alloys," *International Journal of Cast Metals Research,* vol. 13, no. 6, pp. 337-342, 2001.

[41] Sjölander, E., Seifeddine, S., "The heat treatment of Al-Si-Cu-Mg casting alloys," *Journal of Materials Processing Technology,* vol. 210, no. 10, pp. 1249-1259, 2010.

[42] Brooks, C.R., "Heat treating of nonferrous alloys," in *ASM Handbook Volume 4: Heat Treatment*, ASM International, 1991, pp. 1826-2124.

[43] Tavitas-Medrano, F.J., Gruzleski, J.E., Samuel, F.H., Valtierra, S., Doty, H.W., "Effect of Mg and Sr-modification on the mechanical properties of 319-type aluminum cast alloys subjected to artificial aging," *Materials Science and Engineering A,* vol. 480, no. 1-2, pp. 356-364, 2008.

[44] Samuel, F.H., "Incipient melting of Al5Mg8Si6Cu2 and Al2Cu intermetallics in unmodified and strontium-modified Al–Si–Cu–Mg (319) alloys during solution heat treatment," *Journal of Materials Science,* vol. 33, no. 9, p. 2283–2297., 1998.

[45] Han, Y.M., Samuel, A.M., Samuel, F.H., Doty, H.W., "Dissolution of Al2Cu phase in non-modified and Sr modified 319 type alloys," *International Journal of Cast Metals Research,* vol. 21, no. 5, pp. 387-393, 2008.

[46] Chaudhury, S.K., Apelian, D., "Fluidized bed heat treatment of cast Al-Si-Cu-Mg alloys," *Metallurgical and Materials Transactions A: Physical Metallurgy and Materials Science,* vol. 37, no. 7, pp. 2295-2311, 2006.

[47] Moustafa, M.A., Samuel, F.H., Doty, H.W., "Effect of solution heat treatment and additives on the microstructure of Al-Si (A413.1) automotive alloys," *Journal of Materials Science,* vol. 38, no. 22, pp. 4507-4522, 2003.

[48] Crowell, N., Shivkumar, S., "Solution treatment effects in cast Al–Si–Cu alloys.," *AFS Transaction,* vol. 107, p. 721–726, 1995.

[49] Dons, A.L., "The Alstruc homogenization model for industrial aluminum alloys," *Journal of Light Metals,* vol. 1, no. 2, pp. 133-149, 2001.

[50] Sokolowski, J.H., Sun, X.-C., Byczynski, G., Northwood, D.O., Penrod, D.E., Thomas, R., Esseltine, A., "Removal of copper-phase segregation and the subsequent improvement in mechanical properties of cast 319 aluminium alloys by a two-stage solution heat treatment," *Journal of Materials Processing Tech.,* vol. 53, no. 1-2, pp. 385-392, 1995.

[51] Apelian, D., Shivkumar, S., Sigworth, G., " Fundamental aspects of heat treatment of cast Al–Si–Mg alloys," *AFS Transaction,* vol. 137, p. 727–742, 1989.

[52] Zhang, D.L., Zheng, L., "The quench sensitivity of cast Al–7Wt Pet Si–0.4 Wt pct Mg alloy," *Metallurgical and Materials Transactions A ,* vol. 27, p. 3983–3991., 1996.

[53] Seifeddine, S., Timelli, G., Svensson, I.L., "Influence of quench rate on the microstructure and mechanical properties of aluminium alloys A356 and A354," *International Foundry Research,* vol. 59, p. 2–10, 2007.

[54] Rometsch, P.A., Schaffer, G.B., "Quench modelling of Al–7Si–Mg casting alloys," *International Journal of Cast Metals Research,* vol. 12, no. 6, p. 431–439, 2000.

[55] Staley, J.T. , "Quench factor analysis of aluminum alloys," *Material Science and Technology,* vol. 3, pp. 923-935, 1987.

[56] Martin, J.W., "Precipitation hardening," Oxford, UK, Butterworth-Heinemann, 1998, pp. 79-105.

[57] Emadi, D., Whiting, L.V., Sahoo, M., Sokolowski, J.H., Burke, P., Hart, M., "Optimal heat treatment of of A356.2 alloy," *TMS Light Metals,* pp. 983-989, 2003.

[58] Shivkumar, S., Keller, C., Apelian, D., "Aging behavior in cast Al–Si–Mg alloys," *AFS Transaction,* vol. 98, p. 905–911, 1990.

[59] Möller, H., Govender, G., Stumpf, W.E., "Natural and artificial aging response of semisolid metal processed Al–Si–Mg alloy A356," *International Journal of Cast Metals Research,* vol. 20, no. 6, pp. 340-346, 2007.

[60] Reif, W., Yu, S., Dutkiewicz, J., Ciach, R., Krol, J., "Pre-ageing of AlSiCuMg alloys in relation to structure and mechanical properties," *Materials & Design,* vol. 18, no. 11, p. 253–256, 1997.

[61] Gerold, V., In, "Precipitation hardening," in *Dislocations in Solids*, North-Holland, Nabarro, F.R.N. (Ed.). , 1979, p. 222.

[62] Hatch, J.E., "Aluminum: Properties and Physical Metallurgy," Metals Park,OH, ASM, 1984, p. 136–143.

[63] Kang, H.G., Kida, M., Miyahara, H., Ogi, K., "Age-hardening characteristics of Al–Si–Cu-base cast alloys," *AFS Transactions,* vol. 27, p. 507–515, 1999.

[64] Reif, W., Dutkiewicz, J., Ciach, R., Yu, S., Krol, J., "Effect of ageing on the evolution of precipitates in AlSiCuMg alloys," *Materials Science and Engineering A,* Vols. 234-236, p. 165–168, 1997.

[65] Wang, G., Bian, X., Liu, X., Zhang, J., "Effect of Mg on age hardening and precipitation behavior of an AlSiCuMg cast alloy," *Journal of Materials Science,* vol. 39, no. 7, pp. 2535-2537, 2004.

[66] Ouellet, P., Samuel, F.H., "Effect of Mg on the ageing behaviour of Al–Si–Cu 319 type aluminium casting alloys," *Journal of Materials Science,* vol. 34, no. 19, p. 4671–4697, 1999.

[67] Shercliff, H.R., Ashby, M.F. , "A process model for age hardening of aluminium alloys — I. The model," *Acta Metallurgica et Materialia,* vol. 38, no. 10, pp. 1789-1802, 1990.

[68] Cleary, P., Ha, J., Alguine, V., Nguyen, T., "Flow modelling in casting processes," *Applied Mathematical Modelling,* vol. 26, pp. 171-190, 2002.

[69] Kotsiantis, S., Kanellopoulos, D., "Discretization Techniques: A recent survey," *GESTS International Transactions on Computer Science and Engineering,* vol. 32, no. 1, pp. 47-58, 2006.

[70] Mochnacki, B. Suchy, J.S., Numerical Methods in Computations of Foundry Processes, Brzesko: Printgraph, 1995.

[71] Kuzmin, D., " Fakultät für Mathematik," 3 9 2012. [Online]. Available: http://www.mathematik.uni-dortmund.de/~kuzmin/cfdintro/lecture4.pdf. [Accessed 23 6 2012].

[72] Frey, P., "Laboratoire Jacques-Louis Lions," 13 1 2013. [Online]. Available: http://www.ann.jussieu.fr/~frey/cours/UdC/ma691/ma691_ch6.pdf. [Accessed 8 1 2014].

[73] Gustafson, S., "Mathematic Department," 24 1 2012. [Online]. Available: http://www.math.ubc.ca/~gustaf/M31611/fd.pdf. [Accessed 8 1 2014].

[74] Tillová, E., Chalupová, M., Hurtalová, L., "http://www.intechopen.com," 2012. [Online]. Available: http://www.intechopen.com/books/scanning-electron-microscopy/evolution-ofphases-. [Accessed 8 4 2014].

[75] Wang, C.Y., Beckermann, C., "A unified solute diffusion model for columnar and equiaxed dendritic alloy solidification," *Materials Science and Engineering A,* vol. 171, no. 1-2, pp. 199-211, 1993.

[76] Matsumiya, T., Kajioka, H., Mizoguchi, S., Ueshima, Y., Esaka, H., "MATHEMATICAL ANALYSIS OF SEGREGATIONS IN CONTINUOUSLY-CAST SLABS," *Transactions of the Iron and Steel Institute of Japan,* vol. 24, no. 11, pp. 873-882, 1984.

[77] Rometsch, P.A., Arnberg, L., Zhang, D.L., "Modelling dissolution of Mg2Si and homogenisation in Al-Si-Mg casting alloys," *International Journal of Cast Metals Research,* vol. 12, no. 1, pp. 1-8, 1999.

[78] Samuel, A.M., Samuel, F.H, "Modification of iron intermetallics by magnesium and strontium in Al-Si alloys," *International Journal of Cast Metals Research,* vol. 10, no. 3, pp. 147-157, 1997.

[79] Shivkumar, S., Ricci, S., Keller, C., Apelian, D., "Effect of solution treatment parameters on tensile properties of cast aluminum alloys," *Journal of Heat Treating,* vol. 8, no. 1, pp. 63-70, 1990.

[80] Tiryakioğlu, M., Shuey, R.T., "Quench sensitivity of an Al-7 pct Si-0.6 pct Mg alloy: Characterization and modeling," *Metallurgical and Materials Transactions B: Process Metallurgy and Materials Processing Science,* vol. 38, no. 4, pp. 575-582, 2007.

[81] Pedersen, L., Arnberg, L., "The effect of solution heat treatment and quenching rates on mechanical properties and microstructures in AlSiMg foundry alloys," *Metallurgical and Materials Transactions A,* vol. 32, no. 3, pp. 525-532, 2001.

[82] Garcia-Celis, A.I., Velasco, E., Valtierra, S., Mojica, J.F., Colas, R., "Cooling effects on aging in a cast aluminum alloy," in *In Das, S.K. (Ed.), TMS Annual Meeting*, San Antonio, TX, USA, 1998.

[83] Newkirk, J.W., Liu, Q., Mohammadi, A., "Optimizing the aging heat treatment of cast aluminum alloys," in *In: Das, S.K., Skillingberg, M.H. (Eds.), TMS Annual Meeting Automotive Alloys and Aluminum Sheet and Plate Rolling and Finishing Technology Symposia*, Seattle, WA, 2002.

[84] Dobrzañski, L.A., Maniara, R., Sokolowski, J.H., "The effect of cooling rate on microstructure and mechanical properties of AC AlSi9Cu alloy," *Archives of Materials Science and Engineering,* vol. 28, no. 2, pp. 105-112, 2007.